



Yan, Y., Zhang, J., Ince, R. A.A. and Schyns, P. G. (2023) Network communications flexibly predict visual contents that enhance representations for faster visual categorization. *Journal of Neuroscience*, (doi: 10.1523/JNEUROSCI.0156-23.2023).

There may be differences between this version and the published version. You are advised to consult the publisher's version if you wish to cite from it.

<https://eprints.gla.ac.uk/299830/>

Deposited on: 5 July 2023

Enlighten – Research publications by members of the University of Glasgow  
<https://eprints.gla.ac.uk>

---

*Research Articles: Behavioral/Cognitive*

## **Network communications flexibly predict visual contents that enhance representations for faster visual categorization**

<https://doi.org/10.1523/JNEUROSCI.0156-23.2023>

**Cite as:** J. Neurosci 2023; 10.1523/JNEUROSCI.0156-23.2023

Received: 25 January 2023

Revised: 25 May 2023

Accepted: 30 May 2023

---

*This Early Release article has been peer-reviewed and accepted, but has not been through the composition and copyediting processes. The final version may differ slightly in style or formatting and will contain links to any extended data.*

**Alerts:** Sign up at [www.jneurosci.org/alerts](http://www.jneurosci.org/alerts) to receive customized email alerts when the fully formatted version of this article is published.

1       **Network communications flexibly predict visual contents that**  
2       **enhance representations for faster visual categorization**

3  
4       **Abbreviated title: Networks to Predict and Categorize Visual Contents**

5  
6               Yuening Yan<sup>1</sup>, Jiayu Zhan<sup>2</sup>, Robin A.A. Ince<sup>1</sup>, & Philippe G. Schyns<sup>1\*</sup>

7       <sup>1</sup> School of Psychology, University of Glasgow, 62 Hillhead Street, G12 8QB, Glasgow

8       <sup>2</sup> School of Psychological and Cognitive Sciences, Peking University, 5 Yiheyuan Road,  
9       Beijing

10  
11       **\*Corresponding author: Philippe G. Schyns** [Philippe.Schyns@glasgow.ac.uk](mailto:Philippe.Schyns@glasgow.ac.uk)

12       **Keywords:** Brain network; top-down prediction; visual categorization; prefrontal mediation

13       **This manuscript includes** Main Text, Figures 1 to 10, Tables 1 to 2

14       **Number of words:** Abstract (204), Introduction (291), Discussion (1186).

15       **Declaration of interests:** The authors declare no competing interests.

16       **Acknowledgements:** P.G.S. received support from the Wellcome Trust (Senior Investigator  
17       Award, UK; 107802) and the Multidisciplinary University Research Initiative/Engineering and  
18       Physical Sciences Research Council (USA, UK; 172046-01). R.A.A.I. was supported by the  
19       Wellcome Trust [214120/Z/18/Z]. The funders had no role in study design, data collection  
20       and analysis, decision to publish or preparation of the manuscript.  
21

22 **Abstract**

23 Models of visual cognition generally assume that brain networks predict the contents of a  
 24 stimulus to facilitate its subsequent categorization. However, understanding prediction and  
 25 categorization at a network level has remained challenging, partly because we need to  
 26 reverse engineer their information processing mechanisms from the dynamic neural signals.  
 27 Here, we used connectivity measures that can isolate the communications of a specific  
 28 content to reconstruct these network mechanisms in each individual participant (N=11, both  
 29 sexes). Each was cued to the spatial location (left vs. right) and contents (Low vs. High  
 30 Spatial Frequency, LSF vs. HSF) of a predicted Gabor stimulus that they then categorized.  
 31 Using each participant's concurrently measured MEG, we reconstructed networks that  
 32 predict and categorize LSF vs. HSF contents for behavior. We found that predicted contents  
 33 flexibly propagate top-down from temporal to lateralized occipital cortex, depending on task  
 34 demands, under supervisory control of prefrontal cortex. When they reach lateralized  
 35 occipital cortex, predictions enhance the bottom-up LSF vs. HSF representations of the  
 36 stimulus, all the way from occipital-ventral-parietal to pre-motor cortex, in turn producing  
 37 faster categorization behavior. Importantly, content communications are subsets (i.e. 55-  
 38 75%) of the signal-to-signal communications typically measured between brain regions.  
 39 Hence, our study isolates functional networks that process the information of cognitive  
 40 functions.

41

42 **Significant Statement**

43 An enduring cognitive hypothesis states that our perception is partly influenced by the  
 44 bottom-up sensory input, but also by top-down expectations. However, cognitive  
 45 explanations of the dynamic brain networks mechanisms that flexibly predict and categorize  
 46 the visual input according to task-demands remain elusive. We addressed them in a  
 47 predictive experimental design, by isolating the network communications of cognitive  
 48 contents from all other communications. Our methods revealed a Prediction Network that  
 49 flexibly communicates contents from temporal to lateralized occipital cortex, with explicit  
 50 frontal control, and an occipital-ventral-parietal-frontal Categorization Network that  
 51 represents more sharply the predicted contents from the shown stimulus, leading to faster  
 52 behavior. Our framework and results therefore shed a new light of cognitive information  
 53 processing on dynamic brain activity.

## 54 Introduction

55 Since Helmholtz's "unconscious inferences", vision scientists have worked with the  
 56 hypothesis that what we visually perceive is influenced by the bottom-up sensory input, but  
 57 also by top-down expectations of what this input might be (Kinchla and Wolfe, 1979; De  
 58 Lange et al., 2018). Expectations predict upcoming visual information contents (Yuille and  
 59 Kersten, 2006; Friston, 2010; Clark, 2013), thereby facilitating their disambiguation from the  
 60 noisy input (Gilbert and Sigman, 2007; Kok et al., 2012) to speed up categorization behavior  
 61 (Bar et al., 2006).

62 Studies of the dynamic predictive brain have mainly focused on how predictions can top-  
 63 down modulate neural signals. For example, predictions can induce patterns of local  
 64 stimulus-specific activation, in hippocampal, ventral temporal, and primary visual cortex (Kok  
 65 et al., 2014, 2017; Hindy et al., 2016; Margalit et al., 2020), or enhance gamma and reduce  
 66 low-alpha oscillations in visual and frontal cortex (Benedek et al., 2011; Haegens et al., 2011;  
 67 Michalareas et al., 2016; Lobier et al., 2018). Predictions can also enhance high-alpha  
 68 synchronization in the frontal-parietal-occipital network (Lobier et al., 2018). However, key to  
 69 understanding the mechanisms that top-down predict visual contents to facilitate their  
 70 bottom-up categorizations is to reconstruct, from such neural signal modulations, the elusive  
 71 network that process (i.e. predict and categorize) specific information depending on the  
 72 demands of the cognitive tasks. To address these points, we reverse engineered 1) the  
 73 Prediction Network that top-down communicates specific stimulus contents, before the  
 74 stimulus is shown, to the expected contra-lateral occipital hemisphere, and 2) the  
 75 Categorization Network, that bottom-up processes these predicted contents from the  
 76 stimulus to speed up its categorization.

77 Specifically, our research addresses three fundamental information processing questions  
 78 pertaining to the prediction and categorization of visual contents (illustrated in Figure 1):

- 79 1) When, where, and how does a Prediction Network of brain regions flexibly represent  
 80 and communicate the predicted contents of a stimulus?
- 81 2) When, where, and how does a Categorization Network represent and communicate  
 82 these contents when presented in the stimulus for behavior?
- 83 3) How do predicted contents in (1) change stimulus content in (2) to speed up  
 84 categorization behavior?

85

86 [FIGURE 1]

87

## 88 Materials and Methods

### 89 Participants

90 Eleven participants (18-35 years old, mean=26.8, SD=3.0, 4 males and 7 females) took part  
 91 in the experiment and provided informed consent. All had normal or corrected-to-normal  
 92 vision and reported no history of any psychological, psychiatric, or neurological condition that

might affect visual or auditory perception. The University of Glasgow College of Science and Engineering Ethics Committee approved the experiment (Application Number: 300210118).

## Stimuli

Stage 1 of the experimental design (see Figure 2) used two location cues (one for left- and one for right-cued trials). Stage 2 used 3 different sweeping sounds, serving as LSF, HSF and neutral auditory cues. Stage 3 used 2 locations  $\times$  2 spatial frequencies  $\times$  3 orientations Gabor patches as stimuli. We detail them below.

### Stage 1 Location Cues

Participants sat at a 182 cm viewing distance from the screen. We presented a green dot of 1 deg of visual angle diameter for 100 ms to the left (vs. right) of a fixation cross (2 deg of visual angle eccentricity).

### Stage 2 SF Cues

Three 250 ms sweeping sounds started with auditory frequency of 196Hz (cueing LSF), 2217Hz (cueing HSF) or 622Hz (no prediction), with a sweep rate of 0.5 rising octave/second.

### Stage 3 Gabor Stimuli

Left (vs. right)-cued Gabor patches were presented (diameter, 7.5 visual degrees; left and right eccentricity, 12.5 visual degree), with LSF (vs. HSF) contents of 0.5 cycle/degree (vs. 1.2 cycle/degree) shown at one of three randomly chosen orientations (-15 deg, 0 deg, +15 deg). Prior to the task, we calibrated the LSF and HSF Gabor contrast independently for each participant, using an adaptive staircase procedure (target accuracy set at 90%). On each calibration trial, a left (vs. right) green dot presented for 500ms predicted the upcoming left vs. right location of the LSF or (HSF) Gabor patch, itself presented for 100ms. Participants responded “LSF” vs. “HSF” vs. “don’t know” without feedback. We adaptively adjusted LSF vs. HSF contrast as follows:

$$\text{Contrast} = \text{Contrast} - 1 * (\text{Correct vs. Incorrect} - \text{target accuracy}) / \text{Shifting Count},$$

where *Shifting Count* counts the number of direction changes (i.e., increasing to decreasing, or decreasing to increasing). The adaptive staircase stopped when the adjustment step was  $< 0.01$ , setting each SF contrast for this participant’s Gabor stimuli in the actual experiment.

## Procedure

Each three-stage trial started with a central fixation cross presented for 500ms (Figure 2A accompanies the description below):

125

Stage 1. A green dot presented for 100ms appeared to the left or right of the central fixation cross, predicting the left vs. right location of the upcoming Gabor with a validity of 1. This was followed by a jittered blank screen [1000-1500ms].

Stage 2. Three sweeping sounds presented for 250ms predicted the Gabor stimulus presented at Stage 3. On, predictive trials, the 196Hz (vs. 2217Hz) sound predicted the upcoming LSF (vs. HSF) Gabor (both with .9 validity). The 622Hz sound was a neutral cue

without predictive value. This neutral cue was followed by LSF vs. HSF Gabors with .5 probability, on 33% of the trials (neutral trials).

Stage 3. The LSF vs. HSF Gabor stimulus appeared at one of the three rotations on the left vs. right screen location for 100ms. The Gabor was either LSF or HSF, with one of three randomly chosen orientations, followed by a 750 to 1,250ms inter-trial interval (ITI) with jitter. We instructed participants to respond “LSF” vs. “HSF” vs. “Don’t know” as quickly and as accurately as they possibly could. They did not receive feedback. We counterbalanced the use of the three keys (i.e., LSF, HSF, don’t know) across participants, which helped to minimize any effect from specific fingers.

The experiment comprised several blocks of 54 such trials (see Table 1 for details). Participants performed 10-14 blocks in a single day, with short break between blocks. They completed the total of 38-45 blocks over 3-4 days. Participants completed at least 499 trials in each condition (of left vs. right presentation of LSF vs. HSF Gabors). Participants learned the correct relationships between the auditory cues and predicted SF within ~2 blocks of trials, without explicit instructions. We therefore removed these first two blocks from all subsequent analyses.

[TABLE 1]

Auditory localizer. Prior to the experiment, we ran an MEG localizer to model the bottom-up processing of each one of 3 auditory cues. For each cue, each localizer trial started with a blank screen for 500ms, followed by the auditory tone for 250ms, then a blank screen for 1250ms ITI. In a block of 12 trials, 10 of the trials presented the same tone and the two other tones were catch tones. Participants had to press a key whenever the tone was a catch tone. Each participant completed 36 such blocks (i.e., 12 blocks per type of tones), with block order of “low frequency”, “middle frequency”, “high frequency”, repeated 12 times.

#### MEG Data Acquisition and Pre-processing

We measured participants’ MEG activity with a 248-magnetometer whole-head system (MAGNES 3600WH, 4-D Neuroimaging) at a 508Hz sampling rate. We performed the analysis according to recommended guidelines using the FieldTrip toolbox (Oostenveld et al., 2011) and in-house MATLAB code.

For each participant, we discarded the runs (i.e., blocks) with the head movements more than 0.6cm, measured by pre-run vs. post-run head position recordings. We then applied a 1Hz high-pass filter (5<sup>th</sup> order two-pass Butterworth IIR filter) to the remained data, and removed the line noise using discrete Fourier transform. We epoched the raw data into trial windows, separately for each stage: Stage 1, -200ms pre-dot onset to 1,000ms post-dot onset (henceforth [-200ms 1,000ms] around onset); Stage 2: [-200ms 1,000ms] around sweeping sound onset; Stage 3: [-200ms 600ms] around Gabor patch onset. We de-noised the epoched data via a PCA projection of the reference channels. We rejected noisy channels with a visual selection and rejected jump and muscle artifacts with automatic detection (Oostenveld et al., 2011). We decomposed the output dataset with ICA, identified and removed the independent components corresponding to artifacts (eye movements, heartbeat—i.e. 2-4 components per participant).

#### Source Reconstruction

For each participant, we co-registered their anatomical MRI scan with their head shape recorded on the first session and normalized the volume data to standardized MNI coordinate space (Gross, 2019). Using brain surfaces segmented from individual warped MRI, we then prepared a realistic single-shell head model. We resampled each epoched dataset (i.e., each stage) at 512 Hz, low-pass filtered the data at 25 Hz (5<sup>th</sup> order Butterworth IIR filter), specified the time of interest between 0–500 ms (post cue at Stage 2; post Gabor stimulus at Stage 3) and computed covariance across the entire epoch. We then computed the forward model with a 6 mm uniform grid warped to standardized MNI coordinate space, and performed the Linearly Constrained Minimum Variance Beamforming (LCMV) analysis to reconstruct the time series of each source, with parameter 'lambda=6%'. Following the above steps, for each participant we obtained single-trial time series of 4,413 MEG cortical sources at a 512 Hz sampling rate between 0 and 500 ms that we used to analyze the dynamic information processing in the Prediction and Categorization Networks—i.e. at Stages 2 and 3, see Figure 1.

We applied the same pre-processing pipeline to the MEG localizer, using the epoched data [–200 ms–500 ms] around tone onset. We applied the LCMV analysis 0–500 ms post tone, to reconstruct the source representation of the MEG localizer data.

## Analyses

### *Cueing improves behavior*

At a group-level, we discarded invalid predictive trials and applied a 2 (left vs. right location cues) × 2 (valid predictive vs. neutral cueing) × 2 (LSF vs. HSF Gabor patches) ANOVA on the median RTs (excluding incorrect response and outliers) and on the accuracy of all participants. We found a significant main effect of valid predictive vs. neutral SF cueing on RTs, showing that valid predictive trials are significantly faster than neutral trials ( $F(1,10)=20.8$ ,  $p=0.001$ ); and a significant interaction effect between location cue and Gabor SF ( $F(1,10)=17.4$ ,  $p=0.002$ ). Further analysis showed that this predictive vs. neutral cueing effect is significant ( $p<0.05$ , after Bonferroni correction) for each of the 4 experimental conditions (left vs. right locations × low vs. high SFs), quantified by a paired-sample t-test, independently for each condition. For categorization accuracy (ACC), the ANOVA was significant only for valid predictive vs. neutral cueing, showing that ACC is significantly higher in valid predictive than neutral trials ( $F(1,10)=22.5$ ,  $p=0.0008$ ); and a significant interaction between location cue and Gabor SF ( $F(1,10)=13.8$ ,  $p=0.004$ ). Further analysis showed that this effect of SF cue is significant ( $p<0.05$ , Bonferroni correction) for all but the left-LSF experimental conditions (paired-sample t-test independent for each condition).

### *Stage 2: Prediction Network*

#### Prediction representations

To understand the Stage 2 network of regions that propagates the LSF vs. HSF auditory prediction prior to stimulus onset, we computed the representation of the cue across the whole brain, separately for left- and right-cued trials.

For each participant, we computed the single-trial MI (<LSF vs. HSF auditory cue; Stage 2 MEG<sub>t</sub>>), at each time point from 0 to 400 ms following Stage 2 auditory cue onset, on each occipital source (lingual gyrus, cuneus, inferior occipital gyrus), temporal (fusiform gyrus, inferior temporal gyrus, middle temporal gyrus, superior temporal gyrus), parietal (superior



parietal lobe, inferior parietal lobe, angular gyrus, supramarginal gyrus), premotor (precentral gyrus, postcentral gyrus), and frontal (orbitofrontal gyrus, inferior frontal gyrus, middle frontal gyrus, medial frontal gyrus, superior frontal gyrus). We computed MI with the Gaussian Copula Mutual Information (GCMI) estimator (Ince et al., 2017) that supports multi-dimensional variables. This semi-parametric estimator fits Gaussian (maximum entropy) copula, but does not make any assumption about the marginal distributions of the variables.

#### Prediction periods clustering

To compute the number of space x time periods of prediction representations, we applied k-means clustering analysis on all 4413 x 204 (source x time points) dimensional trials as follows:

*Step 1: Peak time extraction.* First, for each participant, and independently for left- and right-cued trials and source, we extracted the peak time MI(<LSF vs. HSF auditory cue; Stage 2 MEG>), 0 and 400ms post auditory cue onset.

*Step 2: Matrix computation.* Across participants and cued conditions, in each ROI (occipital, temporal, parietal, pre-motor and frontal), we summed the numbers of sources that peak during each 10ms-step time window between 0 and 400ms post auditory cue onset (i.e. 39 time windows), producing a 5 (ROIs) x 39 (time windows) matrix of MI peaks. This matrix represented the total brain volume of prediction representation dynamics over time.

*Step 3: Clustering.* We k-means clustered ( $k = 1$  to 30, repeating 1,000 times) the matrix from Step 2, using the 39 time windows as samples and selected  $k$  as the elbow of the within-cluster sums of point-to-centroid distances metric.

The result shows Stage 2, with  $k = 4$  as a good solution, starting with a period 0, before any prediction representation, and then 3 distinct timed periods with temporal, frontal, occipital of peak representations of the prediction.

#### Prediction network nodes (supports Figure 3A)

To reveal the dynamics of MI(<LSF vs. HSF auditory cue; Stage 2 MEG>) representation of the prediction, we localized the source peaking around the first peak in the 90-120ms time window (start), the last peak in 120-200ms (midway) and >200ms (end). We computed the group mean of these 3 source-localized peaks across participants (see Figure 3A for group mean). Further, we applied 2 (left vs. right-cued prediction) \* 2 (left vs. right hemisphere) ANOVA on the prediction representation on occipital sources to test the interaction effect (i.e., the contra-lateral effect).

#### Prediction network reconstruction (supports Figure 3B)

To reconstruct the Stage 2 Prediction Network, we computed Directed Feature Information (DFI, where  $F$  is the auditory cue predicting the upcoming LSF vs. HSF Gabor) in each participant, for each pair of identified network nodes (i.e., sender: temporal, receiver: frontal; sender: frontal, receiver: occipital) as follows:

*Step 1: Source selection.* We selected the highest MI source for the sending and receiving regions in the time window of interest (temporal: 90-120ms, frontal: 120-200ms, occipital: >200ms).

258 *Step 2: Directed Information (DI).* DI (i.e. event-related Transfer Entropy) quantifies  
 259 all the information communicated from sending to receiving sources, removing information  
 260 sent from the receiver itself. For the receiver at time  $x$ , with a communication delay  $y$  from  
 261 the sender, DI is computed as the Conditional Mutual Information (CMI) between  $RA_x$  and  
 262  $SA_{x-y}$  conditioned on  $RA_{x-y}$ :

$$263 \quad DI = CMI\langle RA_x, SA_{x-y} | RA_{x-y} \rangle \quad (1)$$

264 Thus, we computed DI between each sender and receiver source, for each receiver  
 265 time point between 0 and 400ms post auditory cue onset, and for each communication delay  
 266 between 0 and 300ms. This produced the receiver-time  $\times$  transfer-delay DI matrix.

267 *Step 3: DI conditioned on Feature (DI|F).* DI|F removes from DI the information  
 268 communicated about the predictive LSF vs. HSF feature itself. We computed DI|F for each  
 269 receiving-time  $\times$  communication-delay.

270 *Step 4: DFI.* The difference between DI and DI|F isolates the information  
 271 communicated about the predictive cue. We computed DFI as:

$$272 \quad DFI = DI - DI|F \quad (2)$$

273 for each receiving-time  $\times$  communication-delay cell of the matrix.

274 *Step 5: Statistical significance.* We repeated 200 times DFI computations with  
 275 shuffled feature labels (i.e., LSF vs. HSF), using as statistical threshold the 95<sup>th</sup> percentile of  
 276 the distribution of 200 maxima (each taken across the DFI matrix of each shuffled repetition,  
 277 FWER,  $p < 0.05$ , one-tailed).

278 *Step 6: Communication proportions.* To compute the proportion of communications  
 279 about a feature in total network communications between two regions, we computed ratio  
 280  $DFI/DI$ , at the maximum receiving-time  $\times$  communication-delay of the DFI measure.

281 We applied Step 1-6 to reconstruct the Stage 2 Prediction Network of each individual  
 282 participant. Figure 8 shows the individual participants' DFI networks; Figure 3B shows the  
 283 group average network. Note here we established the same statistical significance test for  
 284 each participant and reported a combination of frequentist and Bayesian estimation (Ince et  
 285 al., 2021a). The Bayesian approach contains a two-level analysis, where the first-level  
 286 analysis involves null hypothesis significance testing (NHST) within participants and the  
 287 second level is the Bayesian estimation of population prevalence.

#### 288 Prediction network mediation (supports Figure 4)

289 We then tested whether frontal cortex is a necessary mediator of Stage 2 prediction  
 290 communications between temporal and occipital cortex, by isolating the role of the frontal  
 291 region in these communications. We then compared network communications with and  
 292 without frontal mediation. The steps below detail how we computed frontal mediation in the  
 293 Prediction Network of each participant.

294 *Step 1: Frontal Mediation, DFI.* On the selected temporal and occipital sources, for  
 295 receiving time points between 0 and 400ms post auditory cue onset and for each delay  
 296 between 0 and 300ms, we computed the receiving-time  $\times$  communication-delay of temporal-  
 297 to-frontal DFI and then frontal-to-occipital DFI (each computed as in Prediction network

298 reconstruction). This quantifies the mediating role of the frontal region in the communication  
299 of the predictive cue (cf. Figure 4B).

300 *Step 2: Direct Communication, DFI|Frontal.* To isolate the role of frontal mediation,  
301 we also computed temporal-to-occipital DFI conditioned on the frontal activity. Specifically,  
302 for each time point in the combination of (1) receiving time  $x$  between 0 and 400ms post  
303 auditory cue onset (2) communication delay  $y$  between 0 and 300ms (3) and mediation time  
304  $z$  between receiving time and sending time (i.e.,  $x$  and  $x-y$ ), we computed DFI received by  
305 occipital at time  $x$ , sent by temporal at  $x-y$ , conditioned on frontal activity at time  $z$ . This  
306 produced the 3D DFI receiving-time  $\times$  communication-delay  $\times$  mediation-time conditioned  
307 DFI matrix. We took the minimum conditioned DFI across the mediation time as the directed  
308 communication (i.e., without frontal mediation, Figure 4A).

309 *Step 3: Statistical significance.* We recomputed Steps 1 and 2 and their difference,  
310 shuffling the LSF vs. HSF labels—i.e. 200 repetitions, using the 95<sup>th</sup> percentile of 200  
311 maxima as statistical threshold, each maximum taken across the DFI minus DFI|F matrix of  
312 each shuffled repetition, FWER,  $p < 0.05$ , one-tailed. This isolated the receiving-time  $\times$   
313 communication-delays showing significant enhancement with vs. without frontal mediation.

314 We applied Steps 1-3 to each participant. Figure 4A and B show the results of a typical  
315 participant. Figure 9 shows all individual results. Figure 4C shows the group mean difference  
316 and its Bayesian prevalence.

### 317 **Stage 3: Categorization Network**

#### 318 Stimulus representations

319 To reconstruct the Stage 3 Categorization Network, on predictive trials, we computed for  
320 each participant the dynamics of LSF vs. HSF Gabor stimulus representation across the  
321 whole brain, separately for left- and right-cued trials—i.e. MI(LSF vs. HSF Gabor; Stage 3  
322 MEG), on each source in occipital, temporal, parietal, premotor and frontal regions, at each  
323 time point from 0 to 500ms following Gabor onset.

#### 324 Categorization periods clustering

325 To compute the number of space  $\times$  time stimulus representations period, we applied again k-  
326 means cross-trials clustering analysis on all 4,413 sources  $\times$  256 time points as follows:

327 *Step 1: Peak time extraction.* First, for each participant, and independently for left-  
328 and right-cued trials and source, we extracted the peak LSF vs. HSF representation MI in 50  
329 10-ms time windows spanning 0-500ms post Gabor.

330 *Step 2: Matrix computation.* Across participants and conditions, we counted the  
331 number of sources per ROI (occipital, temporal, parietal, pre-motor and frontal) that peak in  
332 each time window, producing a ROI  $\times$  time matrix of MI peaks.

333 *Step 3: Clustering.* We k-means clustered ( $k = 1$  to 30, repeating 1,000 times) the  
334 matrix from Step 2, using the 50 time windows as samples and selected  $k$  as the elbow of  
335 the within-cluster sums of point-to-centroid distances metric.

336 Stage 3 comprised  $k = 4$  clusters. A first period with no LSF vs. HSF stimulus representation,  
337 followed an occipital-ventral (150-250ms, start), parietal (250-350ms), and premotor-frontal  
338 ( $>350$  ms) periods of stimulus representation.

339 Categorization network nodes (supports Figure 5A)

340 To reveal the dynamics of MI(LSF vs. HSF Gabor; Stage 3 MEG), in each participant, we  
 341 localized the source peaking in each one of the three representational periods. We then  
 342 computed the group mean of these 3 sources across participants. Figure 5A presents the  
 343 group mean.

344 Categorization network reconstruction (supports Figure 5B)

345 To reconstruct the Stage 3 Categorization Network that communicates the Gabor SF across  
 346 occipital, parietal, premotor regions identified earlier, we computed DFI communications of  
 347 the LSF vs. HSF stimulus information. That is, in each participant, for each pair of regions  
 348 (i.e., sender: occipital, receiver: parietal; sender: parietal, receiver: premotor), we performed  
 349 the following three steps.

350 *Step 1: Source selection.* We selected one sender and one receive source with  
 351 highest Stage MI representation of Gabor LSF vs. HSF in the time window of interest  
 352 (occipital: 150-250ms, parietal: 250-350ms, premotor: >350ms).

353

354 *Step 2: DFI.* For each receiver time points between 0 and 500ms post Gabor  
 355 stimulus onset, and for each sender delays between 0 and 300ms, we computed the  
 356 receiver-time  $\times$  communication-delay of LSF vs. HSF stimulus representation with DFI (see  
 357 specific computations in Prediction network reconstruction).

358 *Step 3: Statistical significance* was established recomputing DFI with shuffled LSF vs.  
 359 HSF labels—i.e. 200 repetitions, using as statistical threshold the 95<sup>th</sup> percentile of 200  
 360 maxima, each taken across the DFI matrix of each shuffled repetition, FWER,  $p < 0.05$ , one-  
 361 tailed.

362 *Step 4: Communication proportions.* To compute the proportion of communications  
 363 about a feature in total network communications between two regions, we computed ratio  
 364 DFI/DI, at the maximum receiving-time  $\times$  communication-delay of the DFI measure.

365 We applied Steps 1-4 in each participant, reconstructing the occipital-to-parietal and parietal-  
 366 to-premotor network that communicates the LSF vs. HSF Gabor contents (Figure 10 shows  
 367 all individual results; Figure 5B shows the group average).

368 **Stage 2 to Stage 3: Influences of Prediction Network on Categorization Network**

369 Prediction enhances stimulus representation (supports Figure 6A)

370 To understand how Stage 2 predictions of LSF vs. HSF facilitate their Stage 3 categorization  
 371 when the stimulus is shown, we compared LSF vs. HSF Gabor representations between  
 372 Stage 3 valid predictive and neutral trials, in each participant and Categorization Network  
 373 region (i.e., contra-lateral occipital-ventral, parietal, premotor). Specifically, we computed MI  
 374 as follows:

375 *Step 1: Source selection.* We selected one Stage 3 source per region with highest  
 376 MI(LSF vs. HSF Gabor; Stage 3 MEG<sub>t</sub>) during the time window of interest (occipital-ventral:  
 377 150-250ms; parietal: 250-350ms; premotor: >350ms).

378 Step 2: *MI computation*. For each selected source, we computed source-by-time  
 379 MI(LSF vs. HSF Gabor; Stage 3 MEG), every 2ms between 0 and 500ms post Gabor onset,  
 380 separately for valid predictive and neutral trials. For this computation, we matched number of  
 381 valid predictive trials with neutral trials (random selection). We averaged the MI matrices for  
 382 valid predictive trials from 5 such random trial selections.

383 Step 3: *Statistical significance of difference* was established by recomputing the  
 384 source-by-time MI with shuffled valid predictive and neutral trials (repeated 200 times),  
 385 calculating the difference of peak between recomputed valid predictive and neutral MI in the  
 386 time window of interest, using as statistical threshold the 95<sup>th</sup> percentile of 200 maxima, each  
 387 taken across the source-by-time difference of each shuffled repetition (FWER,  $p < 0.05$ , two-  
 388 tailed).

389 We repeated above Step 1-3 for each participant. Figure 6A shows the group-level results.

#### 390 Prediction modulates Categorization Network source activity and RT (supports Figure 6B)

391 To demonstrate where and when valid predictions modulate premotor MEG activity to  
 392 facilitate behavior, we compared the effect of valid predictive vs. neutral at Stage 2 on Stage  
 393 3 Categorization Network brain activity and behavioral RT.

394 Step 1: *Co-Information*. We computed positive Co-I(<predictive vs. neutral; Stage 3  
 395 MEG<sub>t</sub>; RT>), information theoretic redundancy, as follows:

$$396 \text{ Co-I} = \text{MI}(\text{<predictive vs. neutral; Stage 3 MEG}_t\text{>}) + \text{MI}(\text{<predictive vs. neutral; RT>}) - \\ 397 \text{ MI}(\text{<predictive vs. neutral; Stage 3 MEG}_t\text{, RT>}),$$

398 on every source of the Categorization Network and at every 2ms between 0 and 500ms post  
 399 Gabor onset, producing a vector in Stage 3 time. Specifically, this estimator supports multi-  
 400 dimensional variables, so the joint information MI(predictive vs. neutral; Stage 3 MEG<sub>t</sub>, RT) is  
 401 computed by combining the copula-normalised Stage 3 MEG<sub>t</sub>, and RT variables into a 2d  
 402 variable.

403 Step 3: *Statistical significance* was established by recomputing the Co-I with shuffled  
 404 predictive vs. neutral labels, 200 repetitions, using as statistical threshold the 95<sup>th</sup> percentile  
 405 of 200 maxima, each taken across the vector of each shuffled repetition, FWER,  $p < 0.05$ ,  
 406 one-tailed.

407 We applied Step 1-3 to each participant. Figure 6B shows the group results.

#### 408 **Control Analyses**

##### 409 Stage 1: Dot Representation

410 To check whether representation of the dot cue from Stage 1 remains present until  
 411 representation of the auditory cue in occipital cortex at Stage 2, we computed the dot cue  
 412 representation with MI(<left vs. right dot; Stage 1 MEG<sub>t</sub>>), on each occipital source in lingual  
 413 gyrus, cuneus and inferior occipital gyrus, at each time point (a) from 0 to 1000 ms following  
 414 Stage 1 dot cue onset and (b) from -100ms to 0ms around auditory cue onset at Stage 2.  
 415 We then averaged the time courses of dot representation across the sources. Figure 7A  
 416 shows the results.

##### 417 Stage 2: Auditory Decoding

418 We used classifiers trained on auditory localizer data to cross-decode the bottom-up  
419 processing of the auditory cues at Stage 2 as follows.

420 *Step 1: Training.* We trained linear classifiers (MVPA-Light(Treder, 2020)) to  
421 discriminate the LSF vs. HSF auditory cue, every 2 ms between 0 and 400ms post stimulus,  
422 using MEG sensor responses from the auditory localizer as the training set.

423 *Step 2: Testing.* Every 2 ms between 0 and 400ms post Stage 2 auditory cue, we  
424 computed the classifier decision value from single-trial MEG sensor response. This  
425 produced a 2D (training time  $\times$  testing time) matrix of decision values on each trial. To  
426 quantify decoding performance, across trials we computed for each combination of training  
427 time and testing time the MI between single-trial classification decision value and the true  
428 stimulus label (LSF vs. HSF auditory cue). To establish statistical significance, we repeated  
429 the decoding procedure described 1,000 times with shuffled cue labels, applying threshold-  
430 free cluster enhancement (TFCE(Smith and Nichols, 2009),  $E=0.5$ ,  $H=0.5$ ), and using as  
431 statistical threshold the 95<sup>th</sup> percentile of 1,000 maximum values (each taken across all the  
432 time points per shuffle after TFCE) (i.e., FWER,  $p<0.05$ , one-tailed). We took the maximum  
433 decoding performance across all training time points.

434 *Step 3: Source representation reconstruction.* At the time point of peak performance, for  
435 all 4,413 sources, we computed MI between single-trial decision value and single-trial source  
436 activity.

437 We repeated Steps 1 to 3 to generate the performance curves and source representations of  
438 each participant. Figure 7B averages them across participants.

439

## 440 Results

### 441 1. Prediction speeds up behavior

442 Our three-stage cueing design is depicted in Figure 2A. On each trial, a location cue at  
443 Stage 1 (green dot) briefly displayed left vs. right of a central fixation cross (Posner  
444 cueing(Posner and Petersen, 1990)) predicted the visual hemifield location (left vs. right) of  
445 an upcoming Gabor patch (henceforth, Gabor, see *Methods, Stimuli*) with 100% validity,  
446 followed by a 1-1.5s blank screen. Stage 1 introduced a left vs. right hemisphere task-  
447 demand that a flexible prediction pathway should accommodate. At Stage 2, all trials started  
448 with an auditory cue. On “predictive” trials (66% of total), a 250ms sweeping tone (196 Hz vs.  
449 2217 Hz) signalled the Spatial Frequency content (SF, Low vs. High, with an equal split of  
450 trial numbers) of the upcoming Gabor stimulus with 90% validity. On “neutral” trials (33% of  
451 total), a 622Hz tone had no association with the upcoming stimulus. The auditory cue was  
452 followed by another 1-1.5s blank interval (“prediction period”). Figure 2B depicts the  
453 couplings between auditory cues and Gabors. Finally, at Stage 3, one of two (LSF vs HSF)  
454 Gabor stimuli appeared in the participant’s left or right visual hemifield for 100ms, with fixed  
455 brightness and contrast. Each participant ( $N = 11$ , see *Methods, Participants*) categorized  
456 the Gabor SF as quickly and accurately as they possibly could without feedback (i.e. 3-AFC,  
457 with responses “LSF” vs. “HSF” vs. “don’t know”, see also *Methods, Procedure*).



458

459 [FIGURE 2]

460

461 As expected, SF prediction (in valid, predictive trials) improved categorization accuracy  
 462 (compared to neutral trials), on average by 2.58% (96.9% vs. 94.3%),  $F(1, 10)=22.5$ ,  
 463  $p=0.0008$ , and sped up Reaction Times (RTs), on average by 87.7ms (454.4ms vs.  
 464 542.1ms),  $F(1, 10)=20.8$ ,  $p=0.001$ . Significant RT improvements applied to each Gabor  
 465 location  $\times$  SF presentation condition (see Figure 2C, and Table 2 and *Methods, Cueing*  
 466 *improves behavior*) and individual participant – i.e., Bayesian population prevalence (Ince et  
 467 al., 2021b, 2022), with maximum a posteriori probability (MAP) estimate of the population  
 468 prevalence of the effect of  $11/11 = 1$  (95% highest posterior density interval, HPDI [0.77 1]).  
 469 That is, this experiment provides evidence that this within-participant result generalises to  
 470 most individuals, if they participated in the same experiment.

471

472 [TABLE 2]

473

474 This speeding up of categorization behavior following prediction should involve the  
 475 information processing mechanisms of a flexible, task-demand sensitive Prediction network  
 476 at Stage 2 and a Categorization Network at Stage 3. To understand where, when and how  
 477 their mechanisms led to faster RTs, we reconstructed and analyzed these networks in each  
 478 participant (from 4,413 MEG sources covering the whole brain, see *Methods, MEG Data*  
 479 *Acquisition and Pre-processing*).

480

## 481 2. Prediction Network

482 To identify the brain regions that flexibly communicate the SF prediction over Stage 2, before  
 483 stimulus onset (cf. Figure 1), we computed how strongly each MEG source dynamically  
 484 represents the prediction, separately for left- and right-cued trials at Stage 1 (to reveal  
 485 lateralization of prediction communication into occipital cortex (Flom et al., 1963) at Stage 2).

486 Specifically, for left- and right-cued trials at Stage 1, we computed the Stage 2 spatial-  
 487 temporal representation of the predictive SF auditory cue and MEG source activity using  
 488 Mutual Information (Ince et al., 2017) – i.e. MI (LSF vs. HSF auditory cue; Stage 2 MEG<sub>i</sub>), over  
 489 4,413 MEG sources, every 2ms between 0 and 400 ms post Stage 2 cue onset, see  
 490 *Methods, Prediction representations*. In each participant, this computation produced two  
 491 source-by-time matrices (for left- and right-cued trials at Stage 1) whose MI values indicate  
 492 the strength of SF prediction representation at Stage 2.

493 To reveal the spatial-temporal unfolding of prediction representation, we applied a data-  
 494 driven clustering analysis to these MI matrices (see *Methods, Prediction periods clustering*).  
 495 We found three distinct spatial-temporal periods (i.e. clusters) in both left- (see Figure 3A,  
 496 first row) and right-cued trials (see Figure 3A, second row). Figure 3A summarizes their  
 497 dynamics at group level, by plotting the sources with maximal Stage 2 prediction

498 representation (i.e. peak MI) in each color-coded period. These periods replicated in each  
499 individual participant.

500

501 Specifically, Figure 3A shows that Stage 2 prediction representation dynamics start with an  
502 early Temporal Lobe (TL) peak (auditory cortex, blue, Period 1), moving to prefrontal cortex  
503 (dorsal lateral PFC, [120-200ms], magenta, Period 2), and then finally to the occipital cortex  
504 (OC) contra-lateral to the predicted location ([>200ms], orange, Period 3). Of note, Stage 2  
505 prediction representations were contra-lateralized on occipital sources—i.e. to the Stage 1  
506 cued spatial location, group-level ANOVA, 2 (left vs. right prediction) by 2 (right vs. left  
507 hemisphere occipital cortex),  $F(1, 10) = 18.87$ ,  $p = 0.0015$ , replicated in 10/11 participants,  
508 Bayesian population prevalence = 0.91 [0.64 0.99], MAP [95% HPDI].

509

510 [FIGURE 3]

511

512 The dynamics of prediction propagation suggest a functional network that specifically  
513 communicates the predictive cue. Reconstructing this network requires quantifying the  
514 communication of the predictive information separately from all other communications. We  
515 did this by computing Directed Feature Information (DFI) (Ince et al., 2015a), which  
516 quantifies directed, time-lagged region-to-region communication about a specific feature  
517 (here, the predictive cue). We computed DFI (of LSF vs. HSF prediction, henceforth P)  
518 between pairings of the three sources identified earlier (i.e. one per color-coded period, that  
519 is, temporal, prefrontal and occipital), for each possible time lag, and separately for left- and  
520 right-cued trials—i.e.  $DFI_P(\text{region}A_{t1} \rightarrow \text{region}B_{t2})$ , see *Methods, Prediction network*  
521 *reconstruction*.

522

523 Figure 3B shows these prediction communications as the cross-participant DFI matrix  
524 between sender (y-axis) and receiver sources (x-axis), across different time delays (FWER-  
525 corrected,  $p < 0.05$ , one-tailed), in right-cued trials. The PFC source (x-axis, left panel)  
526 receives the predictive cue ~160ms, sent from the temporal TL source ~50ms earlier (y-axis,  
527 right panel); PFC then flexibly sends the predictive cue (y-axis, right panel) contra-laterally to  
528 left occipital (IOC) sources on right-cued trials (x-axis, right panel), with a 100-200ms delay.  
529 We replicated these communications in individual participants as follows (see prevalence bar  
530 in Figure 3B): TL->PFC: left-cued trials (unfilled) 11/11, right-cued (filled) trials 11/11,  
531 Bayesian population prevalence = 1 [0.77 1] MAP [95% HPDI]; PFC->rOC: left-cued trials,  
532 9/11, Bayesian population prevalence = 0.81 [0.53 0.96], MAP [95% HPDI]; PFC->IOC: right-  
533 cued trials, 10/11, Bayesian population prevalence = 0.91 [0.64 0.99], MAP [95% HPDI], see  
534 Figure 7 for individual results.

535 Importantly, we found that SF communications in the Prediction Network comprise only a  
536 percentage of the total region-to-region communications (calculated by Directed  
537 Information (Massey, 1990), see *Methods Prediction network reconstruction Step 3 and 6*).  
538 These results emphasize the importance of isolating communications of contents—i.e. across  
539 participants,  $74.2 \pm 13.1\%$  of temporal-to-prefrontal for left-cued trials,  $69.4 \pm 19.0\%$  for right-



540 cued trials;  $60.3 \pm 19.0\%$  of prefrontal-to-occipital communications, left-cued trials, and  
 541  $67.1 \pm 22\%$  for right-cued trials.

542 We now know that PFC flexibly communicates the prediction from TL to lateralized OC,  
 543 depending on task-demand stimulus location at Stage 1. We also know that prefrontal cortex  
 544 synchronises with visual cortex (signal-to-signal) in top-down visual predictions tasks (Bar et  
 545 al., 2006; Lobier et al., 2018). Now we test the hypothesis that PFC flexibly mediates the  
 546 communication of prediction contents between TL and OC as a function of task demands. To  
 547 directly test this mediation, Figure 4 contrasts a direct communication of the prediction from  
 548 TL to OC, without (vs. with) PFC mediation—i.e. computing  $DFI_P(TL_{t1} \rightarrow OC_{t3})|PFC_{t2}$ , see  
 549 Figure 4A (vs.  $DFI_P(TL_{t1} \rightarrow OC_{t3})$ , see Figure 4B) and *Methods, Prediction network mediation*.  
 550 Figure 4 reveals that PFC does indeed flexibly mediate the predictive cue from TL to left vs.  
 551 right OC. That is, these communications are conditional on PFC source activity—and  
 552 replicated for left- and right-cued trials in  $\geq 10/11$  participants, see Figure 8, Bayesian  
 553 population prevalence = 0.91 [0.64 0.99] (MAP [95% HPDI]). Thus, PFC actively and flexibly  
 554 mediates the network communications of the prediction from TL to lateralized OC.

555

556 [FIGURE 4]

557

### 558 3. Categorization Network

559 Next, we similarly reconstructed the Stage 3 Categorization Network that processes the  
 560 presented Gabor SF stimulus for behavior. First, on predictive trials, we computed the Stage  
 561 3 dynamic representation of the stimulus to identify space-time regions that represent Gabor  
 562 SF for categorization—i.e. by computing  $MI(\text{Gabor SF; Stage 3 MEG}_t)$ , on each source and  
 563 time point, separately for left- and right-cued trials. Clustering these space-time MI matrices  
 564 revealed again three periods of Gabor stimulus representation (see Figure 5A and *Methods*,  
 565 *Categorization periods clustering*). Specifically, stimulus representation starts with an early  
 566 lateralized occipital-ventral peak ([150-250ms], orange, Period 4), followed by a parietal lobe  
 567 peak ([250-350ms], red, Period 5) and a premotor-frontal cortex peak ( $> 350\text{ms}$ ], brown,  
 568 Period 6), independently for left- and right-cued trials and replicated in all participants—see  
 569 *Methods, Categorization Network, Categorization periods clustering*.

570 Then, we reconstructed in each participant the DFI Categorization Network that  
 571 communicates the LSF vs. HSF contents—i.e., computed as  $DFI(\text{regionA}_{t1} \rightarrow \text{regionB}_{t2})$ , see  
 572 *Methods, Categorization network reconstruction*. Figure 5B shows that these group-  
 573 averaged communications develop from contra-lateral occipital-ventral cortex to parietal and  
 574 then to premotor cortex. We replicated these communications in individual participants as  
 575 follows (see prevalence bar in Figure 5B): rOC->PL, left-cued trials (unfilled) 10/11,  
 576 Bayesian population prevalence = 0.91 [0.64 0.99], MAP [95% HPDI]; IOC->PL, right-cued  
 577 trials (filled) 9/11, Bayesian population prevalence = 0.81 [0.53 0.96], MAP [95% HPDI]; PL-  
 578 >PMC, left- (unfilled) and right-cued (filled) trials 9/11 participants, Bayesian population  
 579 prevalence = 0.81 [0.53 0.96], MAP [95% HPDI], see Figure 9 for all individual results. Here  
 580 again, SF feature communications were a proportion of the total region-to-region network  
 581 communications—i.e.  $56.0 \pm 27.0\%$  of total occipital-ventral to parietal communications, for

left-cued trials and  $62.8 \pm 17.7\%$ , for right-cued trials;  $59.1 \pm 20.5\%$  of total parietal-to-premotor communications for left-cued trials and  $56.2 \pm 23.2\%$ , for right-cued trials.

[FIGURE 5]

#### 4. Stage 2 prediction influences Stage 3 stimulus SF representation for faster categorization

Here, we sought to understand the network mechanisms whereby Stage 2 SF predictions change Stage 3 SF representations from the shown stimulus, leading to faster categorization behavior. We proceeded in two steps, where the first one addresses how prediction changes SF stimulus representation and the second step isolates the Categorization Network components that speed up behavior due to prediction.

##### Step 1. Does prediction enhance SF discrimination for categorization?

We analyzed how Stage 2 SF predictions change Stage 3 stimulus SF representation in each Categorization Network region and participant. Specifically, we computed the difference of SF stimulus representation with and without prediction—i.e. the difference of  $MI(\text{Gabor LSF vs. HSF}; \text{MEG}_{\text{Stage3}})$ , separately computed for valid predictive and neutral trials (see *Methods, Prediction enhances stimulus representation*). These representational differences are presented in the boxplots of Figure 6A, in each color-coded space-time region and participant—i.e. on the source that maximizes the difference in this region, against the null hypothesis of no difference, see 0 dash line. Boxplots show that valid predictions enhanced SF discriminations on occipital-ventral (150-250ms), parietal (250-350ms) and PMC (>350ms) sources, FWER,  $p < 0.05$ , two-tailed. 7/11 participants replicated these results in contra-lateral OC, for left- and right-cued trials, Bayesian population prevalence = 0.64 [0.33 0.85] (MAP [95% HPDI]), 9/11 participants in parietal lobe and PMC, Bayesian population prevalence = 0.81 [0.53 0.96], MAP [95% HPDI] (see prevalence bars in Figure 6A).

##### Step 2. Where and when does prediction speed up behavioral RT in the Categorization Network?

Next, we identified the space-time regions of the Categorization Network that relate to faster Stage 3 RT following Stage 2 prediction. In each participant, we computed the Co-Information(valid predictive vs. neutral cue trials;  $\text{MEG}_{\text{Stage3}}$ ; RT), for each source in the three network regions and separately for left vs. right-cued trials, see *Methods, Prediction modulates source activity and RT*. Co-Information quantifies the influence of prediction that is shared, trial by trial, by MEG and RT. It therefore reveals prediction-related MEG source activity that directly relates to faster RT. Figure 6B plots these results as the participant average of the source with maximal Co-Information at each time point. They reveal two peaks post ~250 ms that maximally relate prediction influence on source activity and faster RT in the Categorization Network at Stage 3. Small brains locate these peaks in the parietal lobe and PMC—replicated in all individual participants, separately for left- and right-cued trials, Bayesian population prevalence = 1 [0.77 1] MAP [95% HPDI].

624 [FIGURE 6]

625

626 In sum, SF Stage 2 predictions enhanced Stage 3 stimulus SF representations in all regions  
627 of the Categorization Network, across the time course of processing, though only the parietal  
628 lobe and premotor cortex speed up RTs.

629

### 630 **Control analyses and Individual results**

631 At Stage 2, besides reconstructing Prediction Network, we additionally conducted analyses  
632 to control for the potential influence from Stage 1 dot presentation to Stage 2 and the  
633 bottom-up processing of the auditory cues. First, we demonstrate in Figure 7A that the Stage  
634 1 dot representation ceases prior to the onset of the auditory cue, providing evidence that  
635 the contra-lateralization observed at Stage 2 is not a residual effect from Stage 1. Equally  
636 importantly, to control for the bottom-up processing of the auditory cues, we traced their  
637 representations at Stage 2 using linear classifier (Treder, 2020) trained to discriminate LSF  
638 vs. HSF auditory cues from localizer data. Figure 7B shows their decoding performance. We  
639 localized the source contributing to the decoding peaks in each time window of the prediction  
640 dynamics. We found that the source representation of the auditory cues remains within TL.

641

642 [FIGURE 7]

643

644 Importantly, we applied a new approach to statistics where we seek to replicate each result  
645 above in each individual participant. We then estimate the Bayesian population prevalence  
646 of the results from the experimental sample of participants, thereby alleviating most  
647 problems of the replication crisis (Ince et al., 2021a, 2022). Having reported the Bayesian  
648 population prevalence, below we show the individual results in detail.

649 We replicated TL->PFC-OC communications in Stage 2 Prediction Network in individual  
650 participants as follows: TL->PFC: left-cued trials (unfilled) 11/11, right-cued (filled) trials  
651 11/11, Bayesian population prevalence = 1 [0.77 1] MAP [95% HPDI]; PFC->rOC: left-cued  
652 trials, 9/11, Bayesian population prevalence = 0.81 [0.53 0.96], MAP [95% HPDI]; PFC->IOC:  
653 right-cued trials, 10/11, Bayesian population prevalence = 0.91 [0.64 0.99], MAP [95% HPDI].

654

655 [FIGURE 8]

656

657 We replicated the result that TL to OC communications are conditional on PFC source  
658 activity for left- and right-cued trials in  $\geq 10/11$  participants, Bayesian population prevalence  
659 = 0.91 [0.64 0.99] (MAP [95% HPDI]).

660

661 [FIGURE 9]

We replicated OC->PL->PMC communications in Stage 3 Categorization Network in individual participants as follows (see prevalence bar in Figure 5B): rOC->PL, left-cued trials (unfilled) 10/11, Bayesian population prevalence = 0.91 [0.64 0.99], MAP [95% HPDI]; IOC->PL, right-cued trials (filled) 9/11, Bayesian population prevalence = 0.81 [0.53 0.96], MAP [95% HPDI]; PL->PMC, left- (unfilled) and right-cued (filled) trials 9/11 participants, Bayesian population prevalence = 0.81 [0.53 0.96], MAP [95% HPDI],

[FIGURE 10]

## Discussion

We isolated the network mechanisms that dynamically predict specific visual contents. Then, we examined specifically where, when and how prediction changes stimulus representation to speed up categorization behavior. Our three-stage experimental design used a location cue to predict the left vs. right visual field location of an upcoming Gabor stimulus at Stage 1, to study the effects of prediction on stimulus representation, specifically in the occipital cortex contra-lateral to stimulus presentation, depending on task demands. The Stage 1 location cue was followed at Stage 2 by an auditory cue that predicted the LSF vs. HSF contents of the upcoming Gabor stimulus that appeared on the screen at Stage 3. We reconstructed a Prediction Network that propagates the auditory predictive cue from temporal (90-120ms post Stage 2 cue) to occipital cortex (200-400ms), via prefrontal cortex (120-200ms), all pre-stimulus. We showed that prefrontal cortex (mainly, dlPFC) mediates communication of the predictive cue from temporal to the left vs. right occipital cortex, depending on cued location at Stage 1, demonstrating that the prediction pathway is flexible depending on the demands of the task. When the Gabor stimulus is finally shown at Stage 3, we reconstructed post-stimulus the Categorization Network that propagates the LSF vs. HSF feature from occipital-ventral cortex (150-250ms post Stage 3 Gabor), parietal lobe (250-350ms post Stage 3 Gabor) and premotor cortex (>350ms post Stage 3 Gabor). We then showed how predictions change the Categorization network and found that they enhance LSF vs. HSF representations of the shown stimulus, from occipital cortex to pre-motor cortex, leading to faster behavior. Together, our results quantitatively reveal cognitive network mechanisms that flexibly communicate top-down the prediction of a specific content to occipital cortex, which enhances the bottom-up representation of these contents in the stimulus to speed up behavior.

### Functional networks predict and then represent stimulus contents

Methodologically, we reconstructed a functional network that flexibly communicates a specific auditory prediction of visual contents (LSF vs. HSF) from temporal to left vs. right occipital cortex, with mediation of the PFC. That is, PFC is necessary to flexibly propagate the predictive cue. Such connectivity analyses involve individual MEG sources acting as sending and receiving network nodes. Importantly, DFI functional connectivity differs from other signal-to-signal connectivity analyses (such as Granger causality or transfer entropy) because DFI isolates what the communication is about (at Stage 2, the auditory prediction of LSF vs. HSF) as a percentage of the full signal-to-signal connectivity (Ince et al., 2015a). At this stage, the specific function of the communications between brain regions that are not about the stimulus features remains to be characterized. They could be about other stimulus

705 features (e.g. its orientation, or contrast), other aspects of the task (i.e. task engagement) or  
 706 related to dynamic state effects (such as attentional engagement or fatigue). Furthermore,  
 707 the remaining communications could relate to the synchronisation between sender and  
 708 receiver nodes that is necessary to form a carrier network to convey the feature information  
 709 (Ziemer and Tranter, 2006; Lobier et al., 2014; Sherblom, 2019).

710 A similar logic isolated the mediatory role of PFC. Thus, DFI addressed the first question  
 711 schematized in Figure 1, of the functional network of regions that dynamically (and multi-  
 712 modally) propagate a prediction of visual information to the PFC that translates a prediction  
 713 from auditory cortex into a predictive signal in occipital cortex that subsequently influences  
 714 the representation of stimulus contents, when shown.

715 These Stage 2 effects were obtained from the contrast between the two auditory cues, and  
 716 therefore might reflect only bottom-up processing of these auditory signals (not the predicted  
 717 visual contents). However, our demonstration that PFC mediates the propagation addresses  
 718 this point, by showing a high-level modulation distinct from the dynamic representation of the  
 719 tone itself (tested with the localizer prior to the experiment, see Figure 7). Also, we proved  
 720 the visual specificity of the Stage 2 prediction with end point in occipital cortex contra-lateral  
 721 to the predicted location (cf. Figure 3). Thus, the propagation of the visual prediction at  
 722 Stage 2 is distinct from that of the auditory input.

723 To address the question of how prediction influences Stage 3 processing of the stimulus, we  
 724 compared Stage 3 stimulus representation with and without prediction. A key unresolved  
 725 question about the role of predictions is whether they enhance vs. dampen stimulus  
 726 representation (De Lange et al., 2018). Evidence for one or the other typically relies on  
 727 enhanced vs. impaired decoding performance of the predicted stimulus in the regions of  
 728 interest (Lee and Mumford, 2003; Kok et al., 2012; Blank and Davis, 2016; Kumar et al.,  
 729 2017). Here, we showed that predictions enhance the representation of LSF vs. HSF  
 730 stimulus contents, locating these enhancements in source space and time. Most participants  
 731 (7/11) showed that prediction enhances LSF vs. HSF discrimination in occipital cortex and  
 732 (9/11) in parietal cortex and (9/11) in premotor cortex, the latter relating to faster behavioral  
 733 categorization. Thus, our evidence supports the hypothesis that prediction enhances  
 734 stimulus representation in the Categorization Network.

### 735 The mediation (i.e. control) role of prefrontal cortex

736 An interesting finding of our functional network is that prefrontal cortex mediates the  
 737 temporal to occipital communication of the predictive cue. More precisely, we located the  
 738 sources with highest representation of the predictive cue in the dorsolateral prefrontal cortex  
 739 (dlPFC, (Sanches et al., 2009)), often related to working memory (D'Esposito et al., 1998;  
 740 Rowe et al., 2000; Friedman and Robbins, 2022), selective attention (Goddard et al., 2022)  
 741 and task performance (Collette et al., 2005). Prefrontal cortex could orchestrate the  
 742 information of the auditory cue (i.e. upcoming LSF vs. HSF) together with the memory of the  
 743 upcoming stimulus location (i.e. left vs. right visual field) and selectively prepare the contra-  
 744 lateral occipital sources to the upcoming contents. Our results are compatible with this  
 745 hypothesis, because representation of the prediction on occipital sources at Stage 2 is  
 746 indeed contralateral to the predicted visual field where the stimulus will appear at Stage 3—  
 747 i.e. left occipital sources for a predicted right visual field stimulus and vice versa. Future work  
 748 that fuses MEG and high-field fMRI will seek to resolve the specific cortical laminar layer that  
 749 receives the prediction at Stage 2 (e.g. central laminar layer (Lawrence et al., 2019)), and

750 how this prediction then interacts with the cortical layer representation of the feedforward  
 751 flow when the stimulus is shown at Stage 3 (e.g. in peripheral laminar layers (Lawrence et al.,  
 752 2019)).

753 *Predictions and representations of face, object, body and scene stimuli.*

754 We used DFI to reconstruct the dynamic Prediction and Categorization Networks. Our  
 755 approach to the neuroimaging of cognitive tasks differs from most other approaches in  
 756 several critical ways. First, our overarching goal is to reconstruct, for each individual  
 757 participant, the network of MEG sources that communicate (i.e. send and receive) the  
 758 information (e.g. an auditory cue; a visual feature) that is necessary to resolve the cognitive  
 759 task under study (Schyns et al., 2009, 2022; Jaworska et al., 2022). These cognitive tasks  
 760 play a critical role to shape the communications of specific stimulus and memory information  
 761 across the networks of the brain (Schyns, 1998; Smith et al., 2004; Jaworska et al., 2022;  
 762 Schyns et al., 2022; Kay et al., 2023). Second, to do so, we use a new measure of functional  
 763 connectivity (i.e. DFI (Ince et al., 2015b, 2016)) that differs from most other signal-to-signal  
 764 measures of connectivity (e.g. Granger causality (Bressler and Seth, 2011) or transfer  
 765 entropy (Lobier et al., 2014)). DFI quantifies communication of specific information between  
 766 network nodes. For example, at Stage 2 of our Experiment, nodes communicate the  
 767 information about the auditory prediction of LSF vs. HSF. DFI communication is expressed  
 768 as a percentage of the full signal-to-signal connectivity between pairs of nodes. With DFI, we  
 769 can uniquely interpret neural signal communications in terms of the specific information  
 770 contents that the brain networks flexibly communicate to achieve a cognitive task. This is  
 771 important to isolate because we showed in our prediction experiment that communications of  
 772 the predicted features is only about 55%-75% of all signal-to-signal communications  
 773 between brain regions. A direct consequence of DFI connectivity is that we can locate the  
 774 network nodes where different information converges (i.e. the hubs—e.g. contra-lateral  
 775 occipital representations of the left and right eyes of a face converge into the right fusiform  
 776 gyrus hub (Schyns et al., 2007; Ince et al., 2016; Zhan et al., 2019; Jaworska et al., 2022)).  
 777 In turn, we can analyze whether hub nodes perform specific linear and nonlinear  
 778 computations on their inputs (Jaworska et al., 2022). And these analyses apply equally to  
 779 bottom-up and top-down information flows in the network. Here, they revealed mechanisms  
 780 that top-down propagate predictions of LSF vs. HSF stimulus feature, from temporal to  
 781 lateralized occipital cortex, depending on task demands. In turn, these predictions enhance  
 782 bottom-up LSF vs. HSF representations, from occipital cortex to pre-motor cortex, to speed  
 783 up categorization behavior. Thus, our approach enables a unique mechanistic, algorithmic  
 784 understanding of the information processing network that realize a specific cognitive task,  
 785 which is the ultimate explanatory goal of cognitiveneuroimaging (Schyns et al., 2009, 2022;  
 786 Jaworska et al., 2022).

787 Generalizing from Gabor stimuli to more naturalistic face, object and scene categorization  
 788 tasks will incur several challenges to study the visual features that categorizes faces, objects  
 789 and scenes (Schyns et al., 2009, 2020). A key challenge is that the stimulus features  
 790 participants use to predict and then categorize can differ across behaviors and levels of  
 791 expertise (e.g. categorizing the same picture as “city” vs. “New York”) (Gauthier et al., 1999;  
 792 Malcolm et al., 2014). We therefore need to characterize these features per participant and  
 793 task to then study their predictions and representations for behavior in functional networks  
 794 (Jaworska et al., 2022; Schyns et al., 2022; Kay et al., 2023). In particular, a methodological  
 795 challenge remains to understand the compositionality of visual predictions, as they



796 decompose from their integrated representation high in the visual hierarchy (e.g., right  
 797 fusiform gyrus), to their contra-lateral components for occipital cortex, down to their simplest  
 798 Gabor representation in the lower hierarchical levels. This would require fusion of brain  
 799 measures (e.g. high-field fMRI to finely tap into laminar layers (Gilbert and Li, 2013) and  
 800 E/MEG (Ince et al., 2015b) to trace the dynamics of these representations across layers in  
 801 the occipito-ventral-dorsal streams).

802 Thus, to understand complex dynamic predictions and representations in the brain, we must  
 803 understand the categorization task (e.g. "city vs. New York"), the hierarchical composition of  
 804 features that represent each category in the participant's memory, trace their hierarchical  
 805 predictions in the feedback flow (Yuille and Kersten, 2006) and their subsequent  
 806 representation in the feedforward flow when the stimulus is shown. Once the  
 807 compositionality of representations is understood, we could study how sensory hierarchies  
 808 decompose predictions to facilitate stimulus processing and behavior.

809

## 810 **Conclusions**

811 We sought to isolate and understand the propagation of specific cognitive predictions in a  
 812 Prediction Network and then how these predictions change the Categorization Network that  
 813 processes the predicted contents in the stimulus. We showed that the Prediction Network  
 814 dynamically propagates predictions of visual contents from temporal to occipital regions, via  
 815 the flexible mediation role of prefrontal regions. Then, we showed that predicted contents  
 816 were more sharply represented when the stimulus is shown in the Categorization Network,  
 817 from occipital-ventral to pre-motor cortex, via parietal cortex, leading to faster decision  
 818 behavior. Our Prediction and Categorization Networks split the communications on specific  
 819 contents from overall signal-to-signal connectivity, in principle generalizing to other stimulus  
 820 features and sensory modalities.

821 **Reference**

- 822 Bar M, Kassam KS, Ghuman AS, Boshyan J, Schmid AM, Dale AM, Hämäläinen MS,  
823 Marinkovic K, Schacter DL, Rosen BR (2006) Top-down facilitation of visual  
824 recognition. *Proc Natl Acad Sci* 103:449–454.
- 825 Benedek M, Bergner S, Könen T, Fink A, Neubauer AC (2011) EEG alpha synchronization is  
826 related to top-down processing in convergent and divergent thinking.  
827 *Neuropsychologia* 49:3505–3511.
- 828 Blank H, Davis MH (2016) Prediction errors but not sharpened signals simulate multivoxel  
829 fMRI patterns during speech perception. *PLoS Biol* 14:e1002577.
- 830 Bressler SL, Seth AK (2011) Wiener–Granger causality: a well established methodology.  
831 *Neuroimage* 58:323–329.
- 832 Clark A (2013) Whatever next? Predictive brains, situated agents, and the future of cognitive  
833 science. *Behav Brain Sci* 36:181–204.
- 834 Collette F, Olivier L, Van der Linden M, Laureys S, Delfiore G, Luxen A, Salmon E (2005)  
835 Involvement of both prefrontal and inferior parietal cortex in dual-task performance.  
836 *Cogn Brain Res* 24:237–251.
- 837 De Lange FP, Heilbron M, Kok P (2018) How do expectations shape perception? *Trends*  
838 *Cogn Sci* 22:764–779.
- 839 D’Esposito M, Aguirre GK, Zarahn E, Ballard D, Shin RK, Lease J (1998) Functional MRI  
840 studies of spatial and nonspatial working memory. *Cogn Brain Res* 7:1–13.
- 841 Flom MC, Heath GG, Takahashi E (1963) Contour interaction and visual resolution:  
842 Contralateral effects. *Science* 142:979–980.
- 843 Friedman NP, Robbins TW (2022) The role of prefrontal cortex in cognitive control and  
844 executive function. *Neuropsychopharmacology* 47:72–89.
- 845 Friston K (2010) The free-energy principle: a unified brain theory? *Nat Rev Neurosci* 11:127–  
846 138.
- 847 Gauthier I, Tarr MJ, Anderson AW, Skudlarski P, Gore JC (1999) Activation of the middle  
848 fusiform ‘face area’ increases with expertise in recognizing novel objects. *Nat Neurosci*  
849 2:568–573.
- 850 Gilbert CD, Li W (2013) Top-down influences on visual processing. *Nat Rev Neurosci* 14:350.
- 851 Gilbert CD, Sigman M (2007) Brain States: Top-Down Influences in Sensory Processing.  
852 *Neuron* 54:677–696.
- 853 Goddard E, Carlson TA, Woolgar A (2022) Spatial and Feature-selective Attention Have  
854 Distinct, Interacting Effects on Population-level Tuning. *J Cogn Neurosci* 34:290–312.
- 855 Gross J (2019) Magnetoencephalography in cognitive neuroscience: a primer. *Neuron*  
856 104:189–204.



- 857 Haegens S, Händel BF, Jensen O (2011) Top-down controlled alpha band activity in  
858 somatosensory areas determines behavioral performance in a discrimination task. *J*  
859 *Neurosci* 31:5197–5204.
- 860 Hindy NC, Ng FY, Turk-Browne NB (2016) Linking pattern completion in the hippocampus to  
861 predictive coding in visual cortex. *Nat Neurosci* 19:665–667.
- 862 Ince RA, Giordano BL, Kayser C, Rousselet GA, Gross J, Schyns PG (2017) A statistical  
863 framework for neuroimaging data analysis based on mutual information estimated via  
864 a gaussian copula. *Hum Brain Mapp* 38:1541–1573.
- 865 Ince RA, Jaworska K, Gross J, Panzeri S, Van Rijsbergen NJ, Rousselet GA, Schyns PG  
866 (2016) The deceptively simple N170 reflects network information processing  
867 mechanisms involving visual feature coding and transfer across hemispheres. *Cereb*  
868 *Cortex* 26:4123–4135.
- 869 Ince RA, Paton AT, Kay JW, Schyns PG (2021a) Bayesian inference of population  
870 prevalence. *Elife* 10:e62461.
- 871 Ince RA, Paton AT, Kay JW, Schyns PG (2021b) Bayesian inference of population  
872 prevalence. *bioRxiv*:2020.07. 08.191106.
- 873 Ince RA, Van Rijsbergen NJ, Thut G, Rousselet GA, Gross J, Panzeri S, Schyns PG (2015a)  
874 Tracing the flow of perceptual features in an algorithmic brain network. *Sci Rep* 5:1–  
875 17.
- 876 Ince RAA, Kay JW, Schyns PG (2022) Within-participant statistics for cognitive science.  
877 *Trends Cogn Sci* Available at:  
878 <https://www.sciencedirect.com/science/article/pii/S1364661322001140>.
- 879 Ince RAA, van Rijsbergen NJ, Thut G, Rousselet GA, Gross J, Panzeri S, Schyns PG  
880 (2015b) Tracing the Flow of Perceptual Features in an Algorithmic Brain Network. *Sci*  
881 *Rep* 5:17681.
- 882 Jaworska K, Yan Y, Van Rijsbergen NJ, Ince RA, Schyns PG (2022) Different computations  
883 over the same inputs produce selective behavior in algorithmic brain networks. *Elife*  
884 11:e73651.
- 885 Kay K, Bonnen K, Denison RN, Arcaro MJ, Barack DL (2023) Tasks and their role in visual  
886 neuroscience. *Neuron* Available at:  
887 <https://www.sciencedirect.com/science/article/pii/S0896627323002180>.
- 888 Kinchla RA, Wolfe JM (1979) The order of visual processing: “Top-down,” “bottom-up,” or  
889 “middle-out.” *Percept Psychophys* 25:225–231.
- 890 Kok P, Failing MF, de Lange FP (2014) Prior expectations evoke stimulus templates in the  
891 primary visual cortex. *J Cogn Neurosci* 26:1546–1554.
- 892 Kok P, Jehee JFM, de Lange FP (2012) Less Is More: Expectation Sharpens  
893 Representations in the Primary Visual Cortex. *Neuron* 75:265–270.
- 894 Kok P, Mostert P, De Lange FP (2017) Prior expectations induce prestimulus sensory  
895 templates. *Proc Natl Acad Sci* 114:10473–10478.

- 896 Kumar S, Kaposvari P, Vogels R (2017) Encoding of predictable and unpredictable stimuli by  
897 inferior temporal cortical neurons. *J Cogn Neurosci* 29:1445–1454.
- 898 Lawrence SJ, Formisano E, Muckli L, de Lange FP (2019) Laminar fMRI: Applications for  
899 cognitive neuroscience. *Neuroimage* 197:785–791.
- 900 Lee TS, Mumford D (2003) Hierarchical Bayesian inference in the visual cortex. *JOSA A*  
901 20:1434–1448.
- 902 Lobier M, Palva JM, Palva S (2018) High-alpha band synchronization across frontal, parietal  
903 and visual cortex mediates behavioral and neuronal effects of visuospatial attention.  
904 *NeuroImage* 165:222–237.
- 905 Lobier M, Siebenhühner F, Palva S, Palva JM (2014) Phase transfer entropy: a novel phase-  
906 based measure for directed connectivity in networks coupled by oscillatory  
907 interactions. *Neuroimage* 85:853–872.
- 908 Malcolm GL, Nuthmann A, Schyns PG (2014) Beyond gist: Strategic and incremental  
909 information accumulation for scene categorization. *Psychol Sci* 25:1087–1097.
- 910 Margalit E, Jamison KW, Weiner KS, Vizioli L, Zhang R-Y, Kay KN, Grill-Spector K (2020)  
911 Ultra-high-resolution fMRI of human ventral temporal cortex reveals differential  
912 representation of categories and domains. *J Neurosci* 40:3008–3024.
- 913 Massey J (1990) Causality, feedback and directed information. In, pp 303–305.
- 914 Michalareas G, Vezoli J, Van Pelt S, Schoffelen J-M, Kennedy H, Fries P (2016) Alpha-beta  
915 and gamma rhythms subserve feedback and feedforward influences among human  
916 visual cortical areas. *Neuron* 89:384–397.
- 917 Oostenveld R, Fries P, Maris E, Schoffelen J-M (2011) FieldTrip: open source software for  
918 advanced analysis of MEG, EEG, and invasive electrophysiological data. *Comput*  
919 *Intell Neurosci* 2011.
- 920 Posner MI, Petersen SE (1990) The attention system of the human brain. *Annu Rev*  
921 *Neurosci* 13:25–42.
- 922 Rowe JB, Toni I, Josephs O, Frackowiak RS, Passingham RE (2000) The prefrontal cortex:  
923 response selection or maintenance within working memory? *Science* 288:1656–1660.
- 924 Sanches M, Caetano S, Nicoletti M, Monkul ES, Chen HH, Hatch JP, Yeh P-H, Mullis RL,  
925 Keshavan MS, Rajowska G, Soares JC (2009) An MRI-based approach for the  
926 measurement of the dorsolateral prefrontal cortex in humans. *Psychiatry Res*  
927 173:150–154.
- 928 Schyns PG (1998) Diagnostic recognition: task constraints, object information, and their  
929 interactions. *Cognition* 67:147–179.
- 930 Schyns PG, Gosselin F, Smith ML (2009) Information processing algorithms in the brain.  
931 *Trends Cogn Sci* 13:20–26.
- 932 Schyns PG, Petro LS, Smith ML (2007) Dynamics of visual information integration in the  
933 brain for categorizing facial expressions. *Curr Biol* 17:1580–1585.

- 934 Schyns PG, Snoek L, Daube C (2022) Degrees of algorithmic equivalence between the brain  
935 and its DNN models. *Trends Cogn Sci*.
- 936 Schyns PG, Zhan J, Jack RE, Ince RA (2020) Revealing the information contents of memory  
937 within the stimulus information representation framework. *Philos Trans R Soc B*  
938 375:20190705.
- 939 Sherblom JC (2019) *Computer-Mediated Communication: Approaches and Perspectives*.  
940 Cognella, Incorporated.
- 941 Smith ML, Gosselin F, Schyns PG (2004) Receptive fields for flexible face categorizations.  
942 *Psychol Sci* 15:753–761.
- 943 Smith SM, Nichols TE (2009) Threshold-free cluster enhancement: addressing problems of  
944 smoothing, threshold dependence and localisation in cluster inference. *Neuroimage*  
945 44:83–98.
- 946 Treder MS (2020) MVPA-Light: a classification and regression toolbox for multi-dimensional  
947 data. *Front Neurosci* 14:289.
- 948 Yuille A, Kersten D (2006) Vision as Bayesian inference: analysis by synthesis? *Trends*  
949 *Cogn Sci* 10:301–308.
- 950 Zhan J, Ince RA, Van Rijsbergen N, Schyns PG (2019) Dynamic construction of reduced  
951 representations in the brain for perceptual decision behavior. *Curr Biol* 29:319-326.  
952 e4.
- 953 Ziemer R, Tranter WH (2006) *Principles of communications: system modulation and noise*.  
954 John Wiley & Sons.
- 955

## 956 Figure Legends

957 **Figure 1. Three key questions. 1) Prediction Network:** Where, when and how does it flexibly  
 958 represent and communicate a predictive cue depending on task demands (here P, an auditory cue  
 959 that predicts a visual content). **2) Categorization network:** When, where and how does it process  
 960 the stimulus contents (here S, the LSF vs. HSF of a Gabor stimulus)? **3) Influence of prediction on**  
 961 **categorization:** How does content prediction influence stimulus representation, leading to faster  
 962 behavior?

963

964 **Figure 2. Experimental design and behavioral results. (A) Task procedure.** Each trial started with  
 965 a 500ms fixation. At Stage 1, a 100ms green dot (i.e. location cue) predicted the left vs. right task-  
 966 demand location of the upcoming Gabor patch, followed by 1000-1500ms blank screen. At Stage 2, a  
 967 250ms sweeping sound (i.e., SF cue) predicted the LSF vs. HSF content of the upcoming Gabor,  
 968 followed by a 1000-1500ms blank screen with jitter. At Stage 3, the Gabor stimulus was presented for  
 969 100ms. Participants categorized its LSF vs. HSF, followed by a 750-1250ms inter-trial interval (ITI). **(B)**  
 970 **Cue-Gabor couplings.** At Stage 1, the left vs. right location cue predicted the left vs. right location of  
 971 the upcoming Gabor with 100% validity. At Stage 2, on predictive trials, the 196 Hz vs. 2217 Hz  
 972 auditory cues predicted the Gabor LSF vs. HSF contents with 90% validity; on neutral trials, a 622 Hz  
 973 auditory cue served as neutral control on 33% of the trials contained no prediction (i.e. with .5  
 974 probability of LSF vs. HSF). **(C) Behavioral results.** Boxplots show that prediction (i.e., valid  
 975 predictive cueing, dark brown) sped up median LSF vs. HSF Gabor categorization RTs in left and  
 976 right-cued trials, compared with neutral cueing (light brown). Black dots (vs. light grey dots) indicate  
 977 the per-participant median categorization RTs in predictive (vs. neutral) trials, linked to show  
 978 directional RT differences replicated in each individual participant.

979

980 **Figure 3. Stage 2 Prediction Network. (A) Network regions (see iconic brain).** In each participant,  
 981 we computed the Stage 2 prediction representation (as MI(LSF vs. HSF cue; MEG), Y-axis), between  
 982 0 and 0.4s post auditory cue (X-axis), on each source, separately for left- and right-cued trials (see  
 983 *Methods, Prediction representations*). We then localized the single source with maximum MI value in  
 984 each color-coded period—i.e. [90-120ms], [120-200ms], [200-300ms], see *Methods, Prediction Network,*  
 985 *Prediction periods clustering*. Glass brains show the cross-participant mean of maximum MI for these  
 986 sources, revealing a temporal sequence of prediction representation propagation from temporal (TL,  
 987 cyan) to prefrontal (PFC, magenta) to occipital (orange, contra-laterally to the left vs. right cued  
 988 stimulus location IOC vs. ROC). **(B) Prediction communications.** For each participant, we used these  
 989 three sources (i.e. one per color-coded period) as the three functional nodes to reconstruct their  
 990 Prediction Network. With DFI (Ince et al., 2015a) we computed the Stage 2 communications of the  
 991 prediction across these three network nodes—i.e. TL->PFC and PFC->OC. Plots show these  
 992 communications averaged across participants, in the time course of the receiving node (X-axis), as  
 993 delays from the sending node (Y-axis)—e.g. TL sends predictive cue P to PFC, with a 50ms delay,  
 994 then PFC sends P to OC, with a 100-200ms delay (as illustrated in the iconic brain below).

995

996 **Figure 4. Prefrontal cortex mediates prediction communication. (A) Direct communication of**  
 997 **the prediction from TL to OC, illustrated in a typical participant.** We removed (i.e. conditioned out) the  
 998 mediation role of PFC in communicating prediction P between TL and lateralized left (l) or right (r) OC.  
 999 The matrices express these P communications in the time course of the receiving IOC source (X-axis),  
 1000 as delays from the sending TL source (Y-axis). **(B) Prefrontal mediation** in communicating P from TL  
 1001 to IOC, with a 100-150 ms delay, illustrated in a typical participant. The significant difference between

(A) Direct and (B) Mediated communications is indicated with a red solid curve in the participant plot (right-cued trials, FWER corrected,  $p < 0.05$ , one-tail). **(C) Group generalization.** The plot shows the cross-participant mean significant difference between (A) Direct and (B) Mediated prediction communication for right-cued trials. The effect replicated in 11/11 participants for left-cued trials (FWER corrected,  $p < 0.05$ , one-tail), Bayesian population prevalence = 1 [0.77 1] MAP [95% HPDI], and in 10/11 participants for right-cued trials, Bayesian population prevalence = 0.91 [0.64 0.99], MAP [95% HPDI]. PFC therefore actively mediates network communications of P from TL to lateralized OC.

**Figure 5. Stage 3 Categorization Network. (A) Network regions (see iconic brain).** In each participant, we computed the Stage 3 Gabor stimulus LSF vs. HSF representation (as MI(LSF vs. HSF Gabor; MEG<sub>i</sub>), Y-axis), between 0 and 0.5s post stimulus (X-axis) on each source, separately for left- and right-cued trials. We then localized the single source with maximum MI value in each color-coded period—i.e. [150-250 ms], [250-350 ms], [≥350 ms]. Glass brains shows the cross-participant mean of maximum MI for these sources, revealing the temporal sequence of stimulus representation propagation starting in contra-lateral occipital-ventral cortex (OC, orange), then parietal lobe (PL, red), and finally premotor and frontal cortex (PMC, brown), independently for left- and right-cued trials. **(B) Stimulus communications.** For each participant, we used these three sources (one per color-coded period) as the three functional sources to reconstruct their Categorization Network. With DFI (Ince et al., 2015a), we computed the Stage 3 communications of Gabor stimulus across these three network nodes—i.e. OC→PL→PMC. Plots show these communications averaged across participants, in the time course of the receiving node (X-axis), as delays from the sending node (Y-axis)—e.g. IOC sends stimulus S contents to PL, with a 100 ms delay (as illustrated in the iconic brain plots below).

**Figure 6. Interaction between Prediction Network (Stage 2) and Categorization Network (Stage 3). (A) Does prediction enhance SF discrimination for categorization?** Boxplots comprise the highest per participant source-level difference of Stage 3 stimulus SF representation—i.e. difference of MI(LSF vs. HSF; MEG<sub>Stage3</sub>) for valid predictive vs. no prediction trials against the null hypothesis of no difference, FWER,  $p < 0.05$ , two-tailed, in each color-coded region and time window (contra-lateral occipital-ventral: 150-250ms; parietal: 250-350ms; PMC: >350ms). These representational enhancements of stimulus SF replicate in each region and time window (see prevalence bar adjacent to boxplots, for left- and right-cued trials). **(B) Where and when does prediction speed up behavioral RT in the Categorization Network?** To identify the Stage 3 Categorization Network regions whose sources relate to faster RTs following valid predictions (vs. no prediction), we computed Co-I(Predictive vs. neutral trials; MEG<sub>Stage3</sub>; RT), FWER-corrected,  $p < 0.05$ , separately for left- (dashed line) and right-cued trials (plain line) on all Stage 3 Categorization Network sources (contra-lateral occipital cortex, parietal lobe and premotor cortex). Plain (right-cued trials) and dashed left-cued trials) curves plot the averages of the per-participant maximum Co-I across sources at each time point. They reveal two sequential peaks post ~250ms, in parietal lobe and pre-motor cortex. Small locate shows the mean Co-I of the individual participant sources that contribute to these peaks.

**Figure 7. Control analyses for Stage 2. (A) Dot representation before auditory cue onset.** For each individual participant, we computed the representation of the dot cue (as MI(left vs. right dot; MEG<sub>i</sub>), Y-axis). We computed the trial-by-trial dot cue representation, by computing MI(<left vs. right dot; Stage 1 MEG<sub>t</sub>>), at each 4ms time point between 0 to 1000 ms following Stage 1 dot cue onset, and also each at time point from -100ms to 0ms before Stage 2 auditory cue onset, on each source in lingual gyrus, cuneus and inferior occipital gyrus. We then averaged time courses of dot representation across the sources. Results show the dot representation ceases prior to the onset of auditory cues. **(B) Auditory processing decoding.** Curves show the auditory decoding performance of the LSF vs. HSF cue, separately for left-cued (upper panel) and right-cued (lower panel) conditions.

We trained classifiers on the auditory localizer to discriminate LSF vs. HSF cue, every 2ms between 0 and 400ms; and tested these classifiers on Stage 2, every 2ms between 0 and 400ms. We quantified the decoding performance (FWER-corrected,  $p < 0.05$ , one-tailed) as MI (classifier decision value; ground truth LSF vs. HSF cue), and took the highest significant performance across training time points. The curve shows the averaged decoding performance across participants – shaded regions denote  $\pm$  standard errors of the mean. Cortical surface maps reveal the MEG sources that contribute to the decoding peaks in each time window of the prediction dynamics, computed as MI(classifier decision value; MEG source activity), indicating the source representation of the auditory cues remains within TL from left hemisphere to the right.

**Figure 8. Stage 2: Communications (DFI) of the LSF vs. HSF prediction in the Prediction Network of individual participants.** Using DFI, separately for (A) left-cued trials and (B) right-cued trials, we computed in each participant (each grey-framed panel) the communications of the prediction across network nodes (i.e. TL  $\rightarrow$  PFC and PFC  $\rightarrow$  OC), every 2 ms between 0 and 400ms post auditory cue onset for the receiver, and every 2 ms communication delay between 0 and 300ms from the sender. These time x time plots represent the significant (FWER-corrected,  $p < 0.05$ ) prediction communications between receiver (X-axis) and sender (Y-axis), where a green diagonal indicates the timing and duration of the prediction communications.

**Figure 9. Stage 2: PFC mediation of prediction communications in the Prediction Network of each participant.** Separately for (A) left- and (B) right-cued trials, we computed the difference of TL to OC Stage 2 prediction communication, between direct (removing frontal mediation) and mediated (with frontal mediation) DFI (for each receiver time point every 2 ms between 0 and 400ms post auditory cue onset, and for each sender communication delay every 2 ms between 0 and 300ms). Each plot presents the significant (FWER-corrected,  $p < 0.05$ , one-tailed) PFC-mediated Stage communication of the cue between TL(Y-axis) and OC (X-axis).

**Figure 10: Stage 3: Communications (DFI) of the LSF vs. HSF Gabor stimulus in the Categorization Network of each participant.** Separately for (A) left- and (B) right-cued trials, we computed in each participant (each grey-framed panel) the DFI communications between categorization network nodes OC  $\rightarrow$  PL and PL  $\rightarrow$  PMC, every 2ms between 0 and 500ms post Gabor onset for the receiver, and for sender communication delays every 2ms between 0 and 300ms. Each plot presents the significant (FWER-corrected,  $p < 0.05$ ) communications of LSF vs. HSF Gabor stimulus between receiver (X-axis) and sender (Y-axis).

1085

1086 **Table 1.** Stimulus repetition in one cueing-categorization block

	Location cue	SF cue	Visual stimuli (random from 3 orientations)
		9 LSF cues	8 left-LSF + 1 left-HSF
Repetitions/type	27 left cues	9 HSF cues	8 left-HSF + 1 left-LSF
		9 neutral cues	9 left-random LSF/HSF
		9 LSF cues	8 right-LSF + 1 right-HSF
	27 right cues	9 HSF cues	8 right-HSF + 1 right-LSF
		9 neutral cues	9 right-random LSF/HSF
Sum		54	

1087

1088

1089 **Table 2.** Group-level effect of cueing on mean LSF vs. HSF, left- and right-cued Gabor  
 1090 categorization RTs (paired samples t-tests).

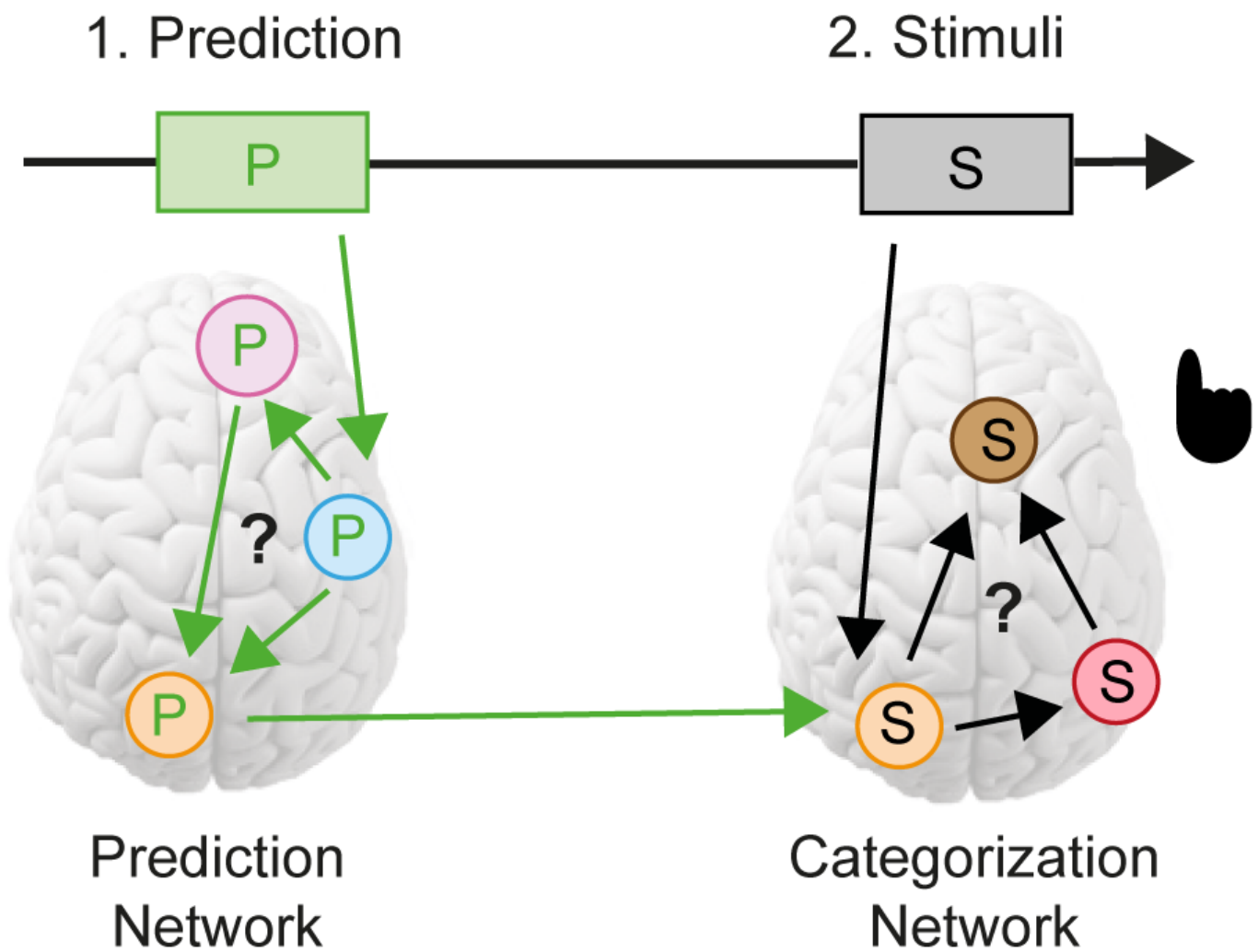
1091

Gabor type	RT (valid predictive, ms)	RT (neutral, ms)	RT Improvement (ms)	<i>t</i> value	<i>p</i> value
Left LSF	530.9	456.8	74.1	$t_{(10)} = 3.60$	$p = 0.005$
Left HSF	555.4	447.7	107.7	$t_{(10)} = 5.87$	$p = 0.0002$
Right LSF	556.3	483.6	72.6	$t_{(10)} = 3.37$	$p = 0.007$
Right HSF	525.9	429.5	96.4	$t_{(10)} = 4.82$	$p = 0.0007$

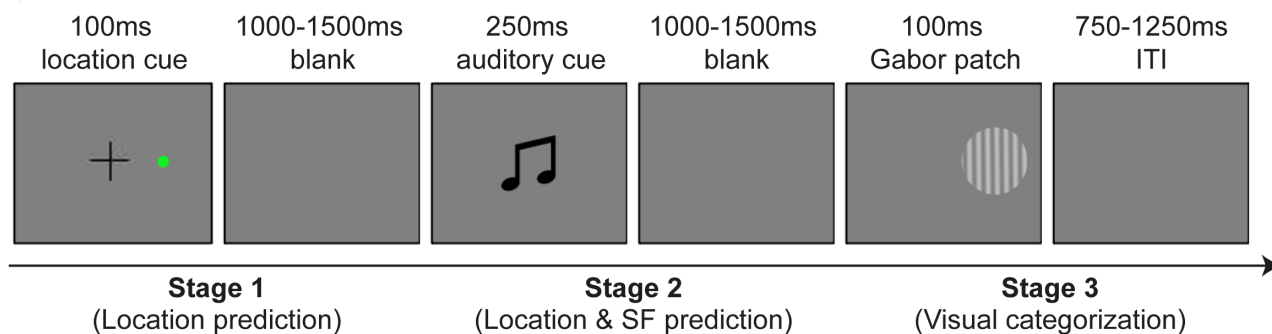
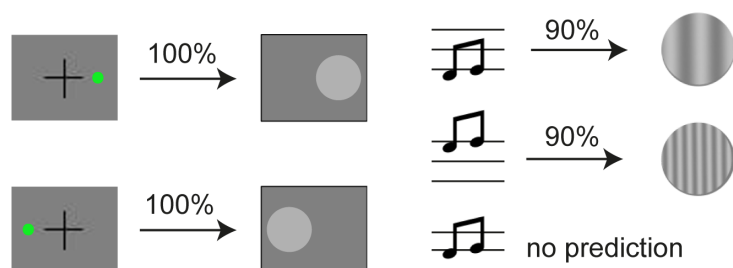
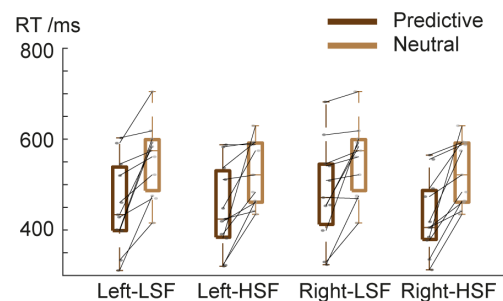
1092

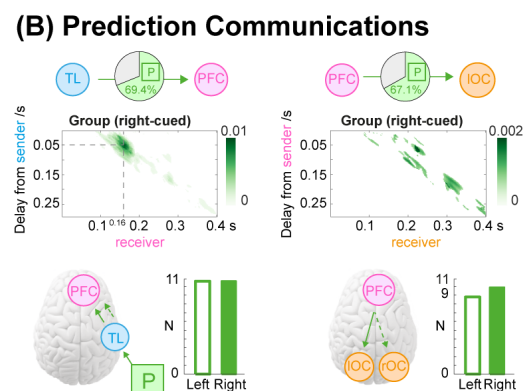
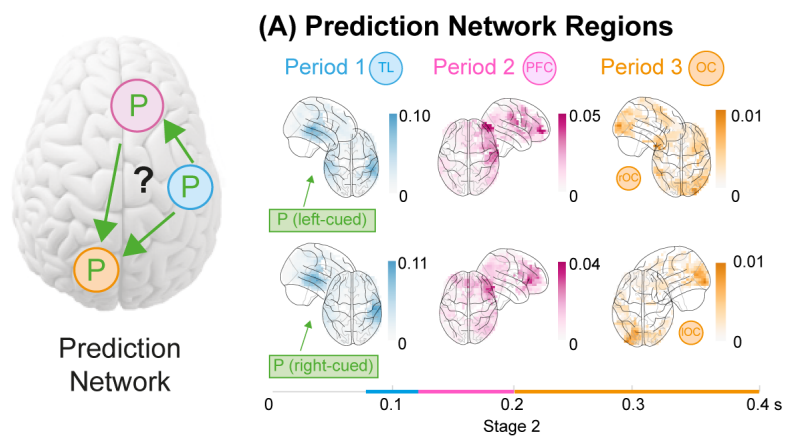


# Communications?

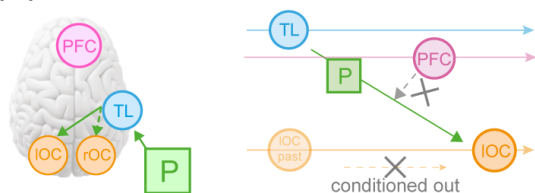




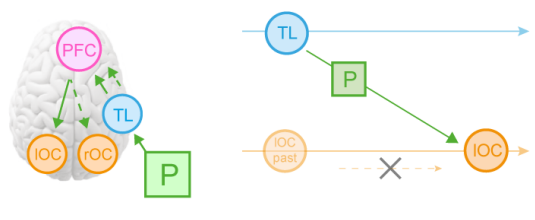
**(A) Task procedure****(B) Cue-Gabor couplings****(C) Behavioral results**



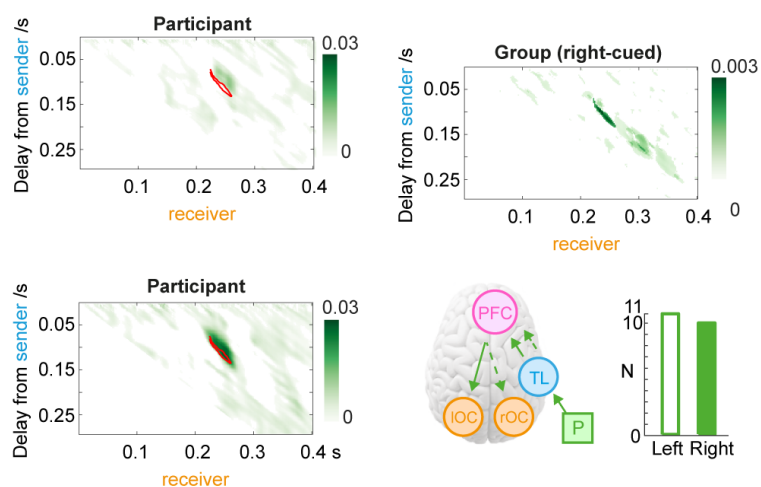
### (A) Direct Communication

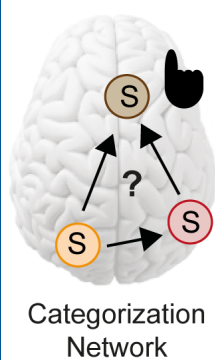


### (B) Prefrontal Mediation

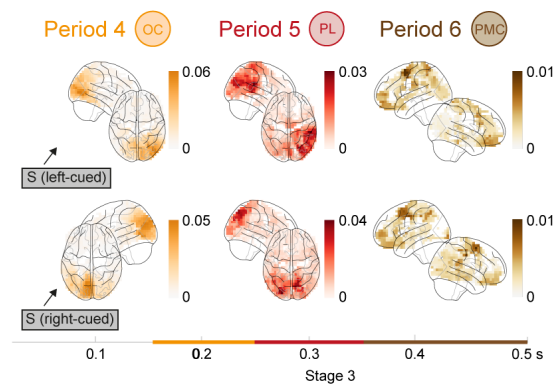


### (C) Group generalization

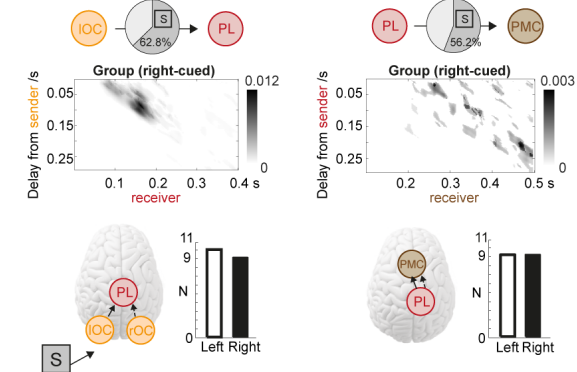


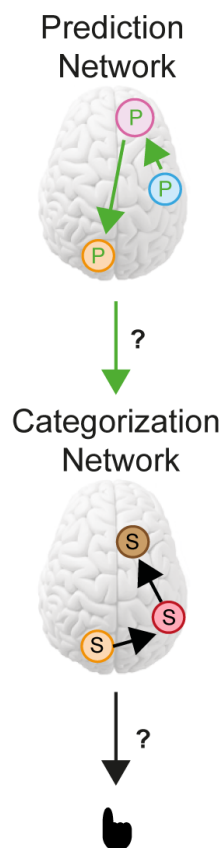


### (A) Categorization Network Regions

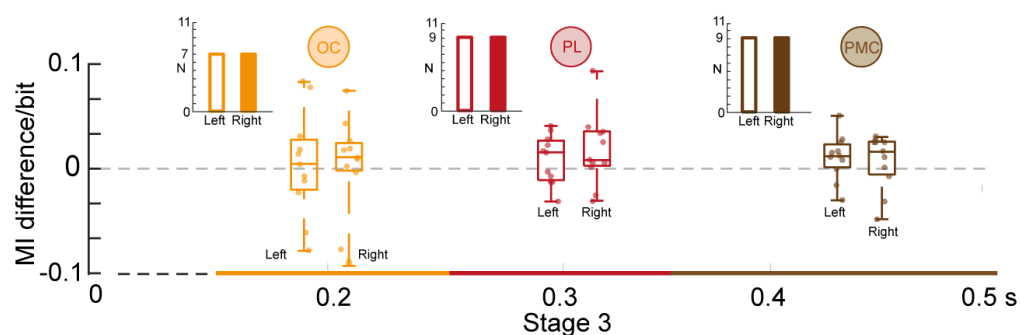


### (B) Stimulus Communications

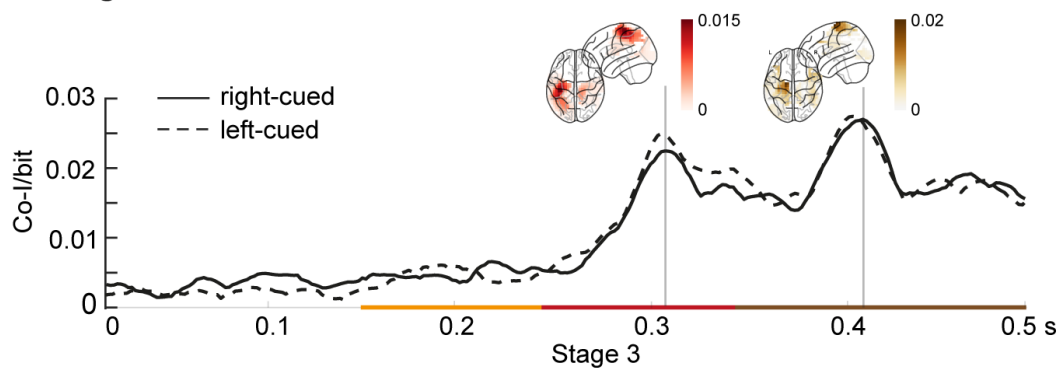




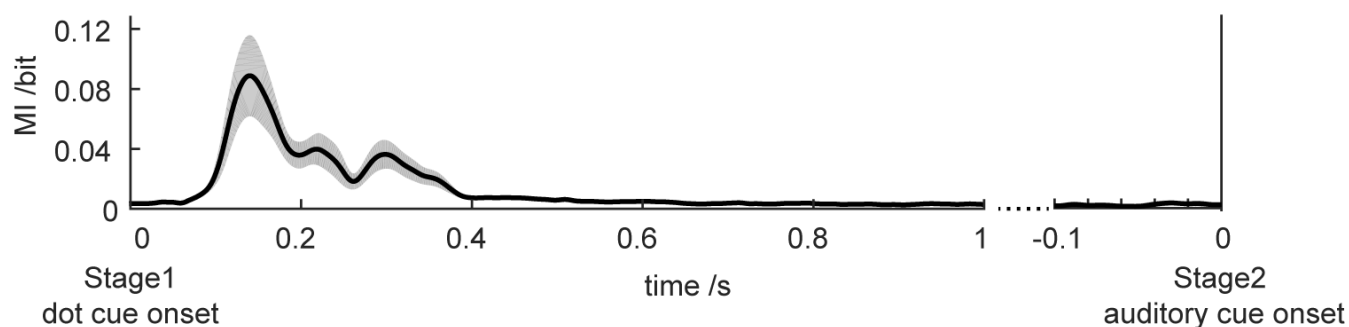
**(A) Does prediction enhance SF discrimination for categorization?**



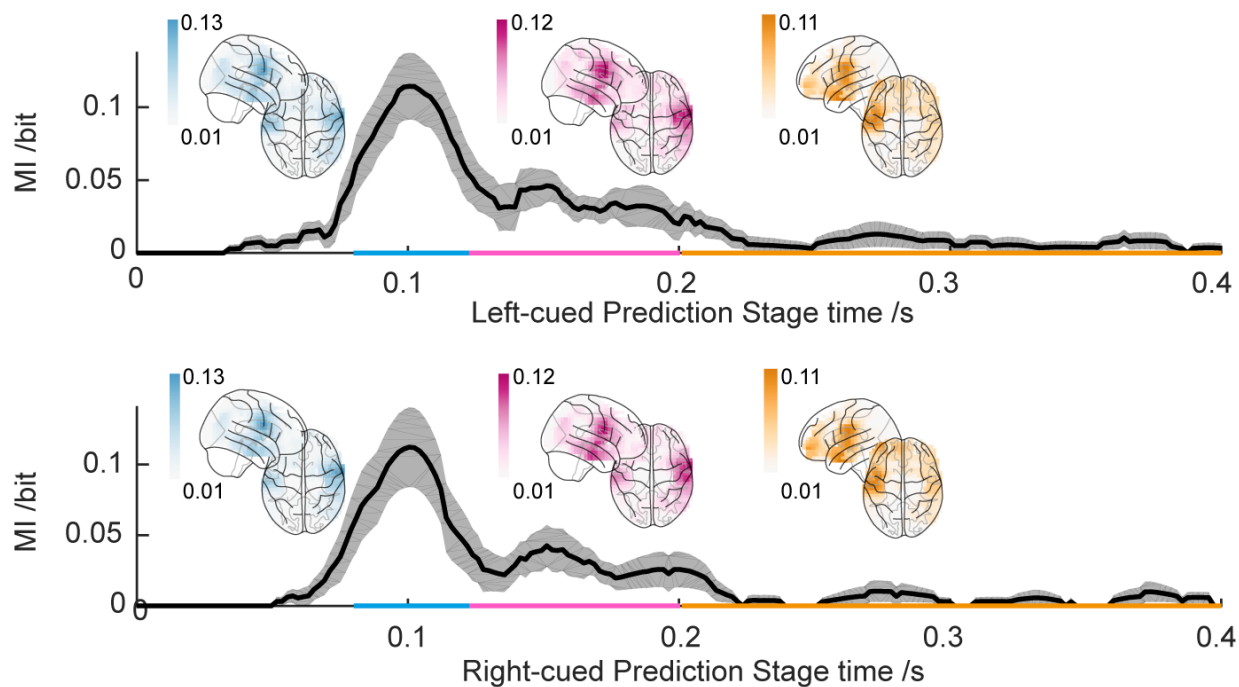
**(B) Where and when does prediction speed up behavioral RT in the Categorization Network?**



### (A) Stage 1 dot representation



### (B) Auditory processing decoding



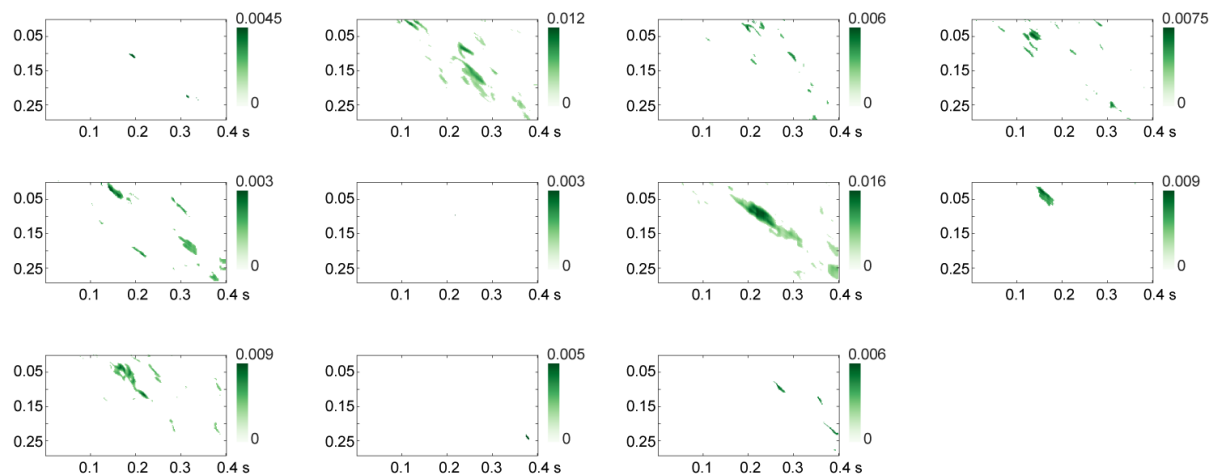
(A) Stage 2 DFI (left-cued trials)



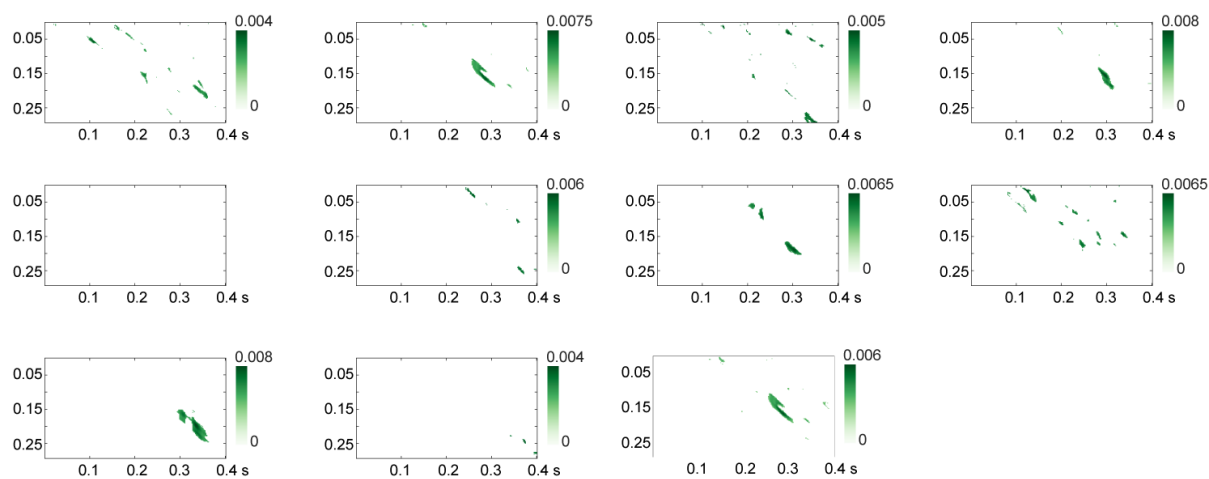
(B) Stage 2 DFI (right-cued trials)



**(A) Stage 2 PFC mediation of prediction communication (left-cued trials)**

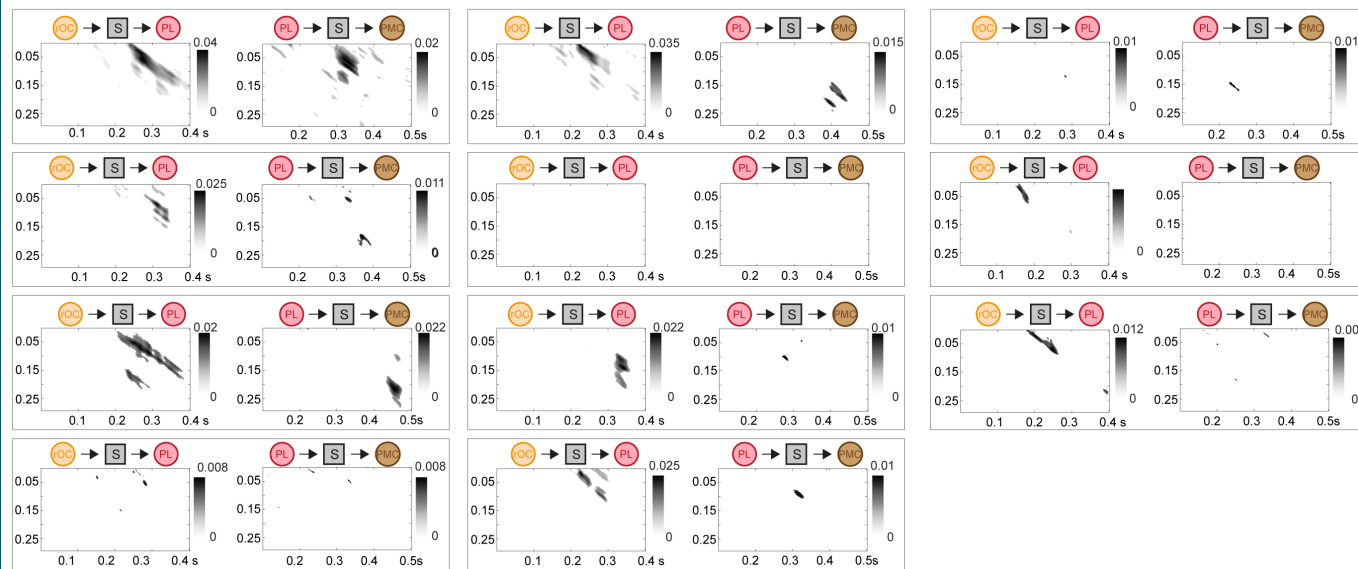


**(B) Stage 2 PFC mediation of prediction communication (right-cued trials)**





(A) Stage 3 DFI (left-cued trials)



(B) Stage 3 DFI (right-cued trials)

